NeuroImage 236 (2021) 118117

Contents lists available at ScienceDirect

NeuroImage

journal homepage: www.elsevier.com/locate/neuroimage

Cortical and subcortical hemodynamic changes during sleep slow waves in human light sleep

Monica Betta[a,1], Giacomo Handjaras[a,1], Andrea Leo[a], Alessandra Federici[a], Valentina Farinelli[b], Emiliano Ricciardi[a], Francesca Siclari[c], Stefano Meletti[b,d], Daniela Ballotta[b], Francesca Benuzzi[b,2], Giulio Bernardi[a,2,*]

[a] MoMiLab Research Unit, IMT School for Advanced Studies Lucca, Piazza San Francesco, 19, Lucca 55100, Italy
[b] Department of Biomedical, Metabolic and Neural Sciences, University of Modena and Reggio Emilia, Modena, Italy
[c] Center for Investigation and Research on Sleep, Lausanne University Hospital, Lausanne, Switzerland
[d] Neurology Dept., Azienda Ospedaliera Universitaria di Modena, Modena, Italy

ARTICLE INFO

Keywords:
Slow wave
NREM
fMRI
EEG
Thalamus
Cerebellum

ABSTRACT

EEG slow waves, the hallmarks of NREM sleep are thought to be crucial for the regulation of several important processes, including learning, sensory disconnection and the removal of brain metabolic wastes. Animal research indicates that slow waves may involve complex interactions within and between cortical and subcortical structures. Conventional EEG in humans, however, has a low spatial resolution and is unable to accurately describe changes in the activity of subcortical and deep cortical structures. To overcome these limitations, here we took advantage of simultaneous EEG-fMRI recordings to map cortical and subcortical hemodynamic (BOLD) fluctuations time-locked to slow waves of light sleep. Recordings were performed in twenty healthy adults during an afternoon nap. Slow waves were associated with BOLD-signal increases in the posterior brainstem and in portions of thalamus and cerebellum characterized by preferential functional connectivity with limbic and somatomotor areas, respectively. At the cortical level, significant BOLD-signal decreases were instead found in several areas, including insula and somatomotor cortex. Specifically, a slow signal increase preceded slow-wave onset and was followed by a delayed, stronger signal decrease. Similar hemodynamic changes were found to occur at different delays across most cortical brain areas, mirroring the propagation of electrophysiological slow waves, from centro-frontal to inferior temporo-occipital cortices. Finally, we found that the amplitude of electrophysiological slow waves was positively related to the magnitude and inversely related to the delay of cortical and subcortical BOLD-signal changes. These regional patterns of brain activity are consistent with theoretical accounts of the functions of sleep slow waves.

1. Introduction

Slow waves of sleep are thought to be crucial for the regulation of several important sleep-related processes, including sensory disconnection and synaptic plasticity related to learning and memory consolidation (Crunelli et al., 2018; Timofeev and Chauvette, 2017; Tononi and Cirelli, 2014). Recent work also suggested that a direct relationship may exist between electroencephalographic (EEG) slow waves, hemodynamic and cerebrospinal fluid (CSF) dynamics, ultimately resulting in the removal of metabolic wastes from the brain (Fultz et al., 2019; Hablitz et al., 2019; Xie et al., 2013).

The appearance of NREM slow waves in the EEG signal depends on the coordinated occurrence of a '*slow oscillation*' (< 1 Hz) in the membrane potential of cortical neurons, between a hyperpolarized *down-state* with neuronal silence and a depolarized *up-state* characterized by intense neuronal firing (Steriade et al., 1993a; Timofeev et al., 2020). While this *slow oscillation* appears in both cortical and thalamic networks, its origin is believed to be cortical. In fact, slow waves persist in the neocortex after thalamic lesions or pharmacological blockade of thalamic activity (David et al., 2013; Steriade et al., 1993). Moreover, slow waves are expressed in isolated cortical slabs in vivo and in cortical slice preparations in vitro (Crunelli and Hughes, 2010; Lőrincz et al., 2015; Sanchez-Vives and McCormick, 2000; Timofeev et al., 2000). On the other hand, the *slow oscillation* disappears in the thalamus of decorticated animals (Timofeev and Steriade, 1996). However, a growing body of evidence indicates that the thalamus and other subcortical structures, including the basal forebrain and several brainstem nuclei, may have an active role in regulating the expression of cortical slow waves in physiological condi-

* Corresponding author.
E-mail address: giulio.bernardi@imtlucca.it (G. Bernardi).
[1] Equal first author contribution.
[2] Equal senior contribution.

https://doi.org/10.1016/j.neuroimage.2021.118117
Received 29 June 2020; Received in revised form 9 April 2021; Accepted 18 April 2021
Available online 30 April 2021

tions (Gent et al., 2018b; Neske, 2016). Indeed, an increase in thalamic activity has been shown to precede the initiation of cortical *up-states* in animal models (Gent et al., 2018a; Sheroziya and Timofeev, 2014; Slézia et al., 2011; Ushimaru and Kawaguchi, 2015). Moreover, thalamic deafferentation of the cortex results in a reduced frequency of the *slow oscillation* (David et al., 2013; Lemieux et al., 2014). Importantly, evidence suggests that subcortical structures may also have a role in triggering the temporally isolated and topographically widespread cortical *down-states* commonly indicated as K-complexes (Cash et al., 2009; Halász, 2016). We recently proposed to name as *type I* the slow waves generated through a subcortico-cortical mechanism, in opposition to *type II* waves that originate spontaneously at cortical level (Bernardi and Siclari, 2019). *Type I* waves, which include evoked and spontaneous K-complexes, especially stand out during light (N2) sleep, when cortical slow waves are still relatively small and sparse (De Gennaro et al., 2000; Siclari et al., 2014).

At the cortical level, each slow wave behaves as a traveling wave characterized by a specific origin and propagation pattern (Massimini et al., 2004; Menicucci et al., 2009; Murphy et al., 2009). Interestingly, slow waves appear to originate more often within the somatomotor cortex and the insula, from which they spread towards anterior and posterior brain areas, especially along the medial surfaces of the two brain hemispheres (Murphy et al., 2009). Such a propagation seems to mostly occur through cortico-cortical white matter connections (Avvenuti et al., 2020; Buchmann et al., 2011; Murphy et al., 2009; Piantoni et al., 2013). Importantly, the organized and systematic traveling of slow waves along connected pathways has been suggested to have an important role in sleep-dependent network-level processes related to plasticity and memory consolidation (Cox et al., 2014; Massimini et al., 2004).

In summary, slow waves of sleep appear to involve complex interactions among multiple cortical and subcortical structures. Understanding such interactions is crucial to improve our knowledge regarding the regulation and functional role of (NREM) sleep, as well as its alterations under pathological conditions. However, conventional EEG investigations in humans have a low spatial resolution and are unable to accurately describe changes in the activity of subcortical and deep cortical structures. These issues may be overcome by combining the optimal temporal resolution of EEG with the high spatial resolution offered by functional magnetic resonance imaging (fMRI; Mullinger and Bowtell, 2010). In fact, one EEG-fMRI investigation on slow-wave correlates reported significant BOLD-signal increases in several brain areas, including the brainstem, cerebellum, inferior frontal cortex, precuneus and posterior cingulate areas (Dang-Vu et al., 2008). Surprisingly, however, no clear changes in thalamic activity were found in association with sleep slow waves. Moreover no cortical regions showed significant decreases in brain activity (but see Czisch et al., 2009, 2002; Laufs et al., 2007) despite the well-known association of slow waves with a highly synchronized suppression of neuronal firing (Steriade et al., 1993). These inconsistencies could have their roots in the non-stationary nature of sleep slow waves, as conventional analyses may fail to capture time-varying changes in brain activity (Mitra et al., 2015). Furthermore, the previous investigation only examined two sub-groups of slow waves, with peak-to-peak amplitude in the range 75–140 μV or lager than 140 μV, and was thus unable to determine how relative variations in slow-wave amplitude relate to changes in hemodynamic activity measured through fMRI. In order to address these issues, here we took advantage of simultaneous EEG-fMRI recordings to obtain spatially and temporally detailed maps of cortical and subcortical hemodynamic fluctuations time-locked to sleep slow waves (0.5–2 Hz), operationally defined as negative half-waves of any amplitude (Bernardi et al., 2018; Valomon et al., 2021), with a duration of 0.25–1.0 s (0.5–2 Hz), detected during any of the stages of NREM sleep (N1/N2/N3). In particular, here we analyzed data collected during an afternoon nap session, which mainly included light sleep dominated by K-complexes and isolated slow waves.

2. Materials and methods

2.1. Participants

Twenty healthy adult volunteers (age 29.7 ± 3.9 years, range 25–42; 11 females; all right-handed) participated in the study. A clinical interview was performed to rule out history or presence of any disorder that could significantly affect brain function. Then, recruited participants underwent simultaneous EEG-fMRI recording during an afternoon nap opportunity. In order to facilitate transition into sleep during the scan session, subjects were asked to wake-up 1 to 2 h earlier than usual in the morning of the experiment and to restrain from consuming caffeine-containing beverages in the few hours that preceded the scan session. On average, participants reported to have slept for 4.9 ± 1.5 h the night before the experiment, which corresponded to 66.2 ± 26.3% of their usual sleep time.

As detailed below, we also re-analyzed waking resting state (rs-)fMRI (no EEG co-acquisition) and sleep hd-EEG data collected in two independent samples of healthy adult individuals. Specifically, rs-fMRI data was obtained in a group of 28 adult subjects (age 25.0 ± 5.3 years, range 19–43; 14 females; 14 left-handed). Data acquisition was performed using the same MRI scanner and acquisition parameters comparable to those employed in the present study. This dataset was used to generate thalamic and cerebellar functional connectivity maps (see below). The hd-EEG data consisted of overnight sleep recordings obtained at the University Hospital of Lausanne (Switzerland) in a distinct set of 12 healthy adult volunteers (age 25.5 ± 3.7 years, 6 females) who participated in a larger project aimed at exploring the effect of visual experience on sleep slow waves (Bernardi et al., 2019a). Here we only included data from the control condition, in which subjects remained in the sleep laboratory and watched movies of their choice (selected from a pre-defined list) from 3 to 8PM. This dataset was used to generate a map of EEG slow-wave propagation in source space (see below).

All experiments were conducted under protocols approved by the respective Local Ethical Committees, in accordance with the ethical standards of the 2013 Declaration of Helsinki. Written informed consent was obtained from all participants.

2.2. Data acquisition

All study participants underwent simultaneous EEG, ECG and fMRI recordings during an afternoon nap opportunity (2:30–4:00PM). Custom-made foam pads were used to improve the comfort of the subjects inside the coil and minimize possible head movements. The participants received instruction to relax and try to sleep in the scanner. The study was interrupted after acquisition of five 10-min fMRI runs or when the participant started to feel uncomfortable in the scanner and/or felt unable to fall asleep. Of note, here we chose to use brief runs rather than a single long run because continuous scanner operation is associated with a relevant B_0 field drift (in part cause by heating; Foerster et al., 2005), which is expected to increase if the cooling pump is turned off, as in most EEG-fMRI studies (van der Meer et al., 2016). In this respect, the presence of periodic interruptions in data acquisition allowed the occurrence of automated adjustments of the magnetic field and favored a minimal cooling-down of the scanner between sessions, thus preserving as much as possible the quality of fMRI data. Importantly, pilot studies were performed to ensure that both the noise produced during scan sessions and the noise changes during breaks between runs were well tolerated and not associated with frequent awakenings.

The EEG was recorded using an MR-compatible EEG cap (Micromed, Mogliano Veneto, Italy) including 32 electrodes online-referenced to FCz (1024 Hz sampling frequency). The electrode-skin impedance was brought below 10 KΩ at the beginning of the scan session. During simultaneous EEG-fMRI acquisition, electrophysiological data were transmitted through a fibreoptic cable from the high-input impedance amplifier (22 bits resolution, with range ± 25.6 mV) in the scanner room to

a computer located outside. Before transmission, the signal was band-pass filtered between 0.15 and 269.5 Hz by an anti-aliasing hardware band-pass filter.

Functional and anatomical data were acquired using a 3T Philips Achieva MR-scanner. T2*-weighted gradient-echo echoplanar sequences were used to acquire functional data from 39 axial contiguous slices (300 vol per run; TR = 2000 ms; TE = 35 ms; FA = 80°; voxel size: 3 × 3 × 3 mm). The scanner cooling-pump and the ventilation fans were turned off during data acquisition as they may generate artifacts in the EEG signal (Nierhaus et al., 2013). Moreover, MRI volume acquisition markers were sent to the EEG recording system via a dedicated trigger cable, thus ensuring synchronization between fMRI and EEG data. A high-resolution T1-weighted MPRAGE anatomical image was also obtained at the end of the experimental session. The volume consisted of 170 sagittal slices (TR = 9.9 ms; TE = 4.6 ms; in plane matrix = 256 × 256; voxel size = 1 × 1 × 1 mm).

2.3. EEG data preprocessing and analysis

All EEG recordings were preprocessed in MATLAB (The MathWorks, Inc.) using EEGLAB (Delorme and Makeig, 2004). The FMRIB-plugin (Iannetti et al., 2005; Niazy et al., 2005) was used to remove fMRI-related artifacts from EEG data through the following steps: removal of MR gradient artifacts based on average artifact subtraction (AAS), subtraction of the principal components (PC) of artifact residuals (Optimal Basis Sets method; OBS) and adaptive noise cancelation (ANC); signal down-sampling to 256 Hz; automated detection of QRS complexes in ECG channel followed by removal of ballistocardiographic artifacts (i.e., artifacts caused by cardiac pulse-related movement of the scalp electrodes inside the magnetic field; Allen et al., 2000) based on subtraction of PCs of artifact residuals (OBS). In brief, the gradient artifact was removed using the FMRI Artifact Slice Template Removal (FASTR) tool, which calculates an average template gradient artifact, subtracts this template from the data, and then uses PCA to remove up to 90% of the residual artifact. The ballistocardiographic artifact was removed using a similar method. Of note, all automated QRS detections were visually inspected and wrong or missing markers were manually corrected using custom-made MATLAB functions. Finally, EEG recordings were band-pass filtered between 0.5 and 18 Hz and an Independent Component Analysis (ICA; Delorme and Makeig, 2004) was applied to remove any residual activity of artifactual origin, including artifacts related to eye movements and muscular activity. This procedure has been shown to reduce the impact of EEG artifacts on power computation and on the identification of individual graphoelements while producing negligible changes in physiological signals of interest (Iriarte et al., 2003; Romero et al., 2003). Bad channels were visually identified, rejected and interpolated using spherical splines from the activity of the nearest sensors.

The EEG signal was re-referenced to the average of channels T5 and T6 (representing the closest electrodes to the ASSM-recommended mastoid references), and sleep scoring was performed over 30-s epochs according to standard criteria (Iber et al., 2007). Data-segments containing residual artifactual activity (e.g., due to muscular and ocular activity during arousals, or spikes caused by a non-perfect elimination of gradient or ballistocardiographic artifacts) were manually marked through visual inspection and excluded from further analyses as detailed below. The negative-going signal envelope was calculated as described in previous work prior to application of a validated slow wave detection algorithm (Mensen et al., 2016). In particular, for each time-point, the four most negative samples (electrodes) were selected and averaged after discarding the single most negative sample. This approach was used to minimize the potential impact of any residual large-amplitude artifactual activity in isolated electrodes. The resulting signal was baseline corrected (zero mean-centered) prior to the application of a negative-half-wave detection procedure based on the identification of consecutive signal zero-crossings (Riedner et al., 2007; Siclari et al., 2014). Differently from commonly applied channel-by-channel detection approaches, this method allows for the identification of both local and widespread slow waves and to define a unique time reference (across electrodes) for each negative wave (Mensen et al., 2016). Only negative half-waves detected during NREM sleep epochs (N1/N2/N3) and with a duration comprised between 0.25 s and 1.0 s (full-wave period 0.5–2.0 s, corresponding to a 0.5–2.0 Hz frequency range) were selected for subsequent analyses. An amplitude threshold was not applied. Of note, however, the adopted detection approach tends to underestimate slow-wave amplitude at the level of individual electrodes and thus intrinsically 'filters out' small-amplitude waves/oscillations (Mensen et al., 2016). The timing of the first zero-cross (from positive to negative) was used as a reference to mark the beginning of each slow wave (slow-wave onset). Moreover, the amplitude (A; unit: μV), defined as the absolute value of the maximum negative peak, and the zero-cross-to-negative-peak time (d_1; unit: s) of all detected half-waves were computed and stored for further analyses.

Given that sleep spindles (10–16 Hz) may commonly occur in association with slow waves, specific analyses were performed to evaluate the impact of modeling spindles on hemodynamic signal changes (see below). To this aim, the onset time and duration of sleep spindles were identified from the EEG time-series of channel Cz (Schabus et al., 2007) using a validated algorithm (Mensen et al., 2018; Wamsley et al., 2012). In brief, a wavelet-based filter (10–16 Hz) was applied to the EEG time-series using a b-spline wavelet (Lajnef et al., 2015), and the power of the resulting signal was measured by squaring the values and smoothing the time-series using a sliding window of 100 ms. Then, potential spindles were defined as points in which power values passed a high-threshold corresponding to the median plus 4 times the median absolute deviation (MAD) of signal power. The actual start and end points of identified events were then measured using the crossing-times at a second, low-threshold corresponding to the median power plus 2 MADs. The thresholds were re-computed for each 30 s epoch. Only events with duration comprised between 0.3 and 3 s and detected during N2/N3 sleep or transitional N1 epochs (i.e., N1 epochs adjacent to N2/N3 epochs) were retained for further analysis. Finally, a power-ratio threshold was applied in order to ensure some specificity of the transient power increases within the spindle range. Specifically, for each potential spindle we computed the ratio of the mean power in the spindle range over the mean power in the neighboring ranges (8–10 Hz and 16–18 Hz) and we eventually retained the detected event if the obtained value was greater than 3.

2.4. MRI data preprocessing and analysis

Functional MRI data were preprocessed using *AFNI* (Cox, 2012, 1996). First, signal outliers were removed from single-voxel time-series (*3dDespike*) and the time-shift related to slice acquisition was corrected (*3dTshift*). Data from different runs were then registered to a reference volume for motion correction (*3dvolreg*) and spatially smoothed (*3dBlurToFWHM*) with a 6 mm full-width-at-half-maximum (FWHM) Gaussian kernel. For each fMRI run, the signal of each voxel was converted to percent BOLD-signal change with respect to the mean BOLD-signal across the corresponding run. Additional preprocessing steps were performed to remove potential artifactual components in the fMRI signal. In particular, the BOLD-signal from each voxel was cleaned by regressing-out (*3dREMLfit*) head-motion parameters, movement spike regressors (frame wise displacement above 0.3) and the mean signal of cerebro-spinal fluid (CSF; Duyn et al., 2020), as well as accounting for the temporal autoregression (*ARMA-1*), which typically reflects artifacts of physiological origin (Bright et al., 2017). The pre-processed data were then non-linearly transformed (*3dNwarpApply*) into the Montreal Neurological Institute (MNI152) coordinate system and resampled to a 2 mm isovoxel resolution. Finally, to reduce computational effort in the subsequent steps, a gray matter spatial mask was also applied ($p > 0.10$ in the tissue probability map of the ICBM 2009c atlas; Fonov et al., 2009).

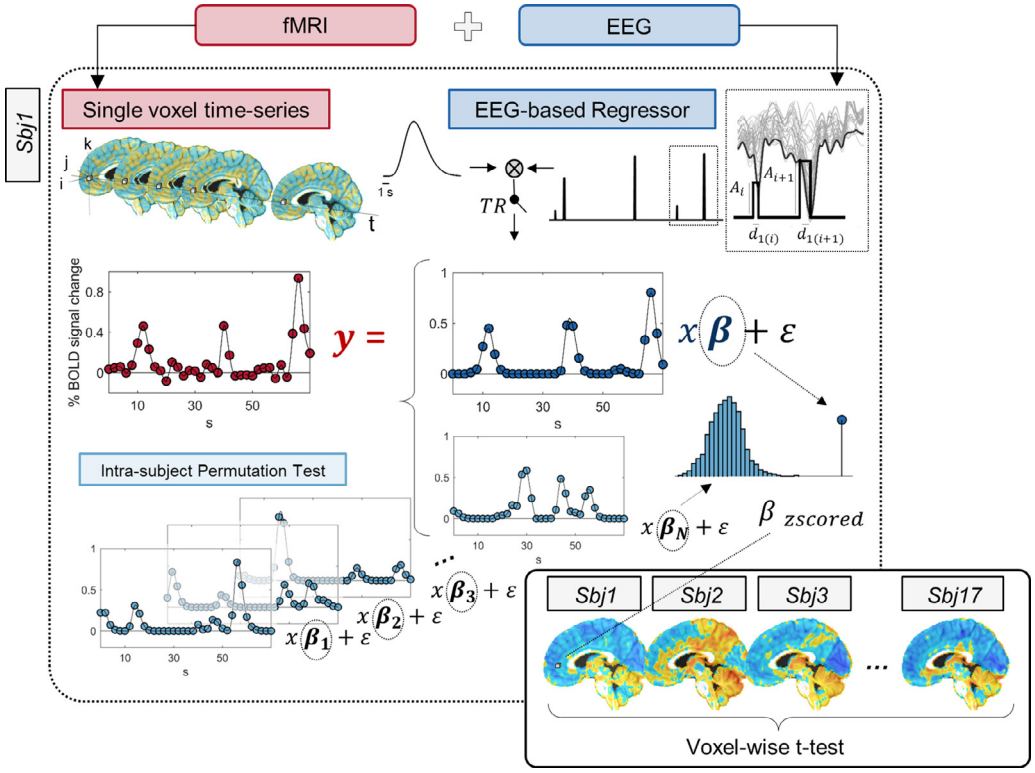

Fig. 1. Schematic representation of procedures applied for the voxel-wise regression analysis. Each slow wave was modelled as a square wave with onset-time corresponding to the timing of the first zero-crossing, height equal to the absolute value of the maximum negative amplitude of the slow wave (A), and duration corresponding to the duration of the descending phase of the wave (d1). The obtained regressor was then convoluted with a standard gamma hemodynamic response function (HRF), down-sampled to the fMRI sampling rate and used to regress the BOLD time-series from each voxel. At single-subject level, beta-values of each voxel were converted into z-scores calculated with respect to a null distribution obtained by re-computing the regression after shuffling the timing of individual slow waves (nPerm =1000). A one-sample *t*-test was performed to assess statistical significance at group-level.

Brain regions associated with the occurrence of sleep slow waves were identified through a voxel-wise regression of BOLD time-series (Fig. 1). Specifically, for each subject, an EEG-based regressor was built, in which each slow wave was modelled as a square wave with onset-time corresponding to the timing of the first zero-crossing of the negative half-wave, height equal to the absolute value of the maximum negative peak (A), and duration corresponding to the length of the descending phase of the wave (from first zero-crossing to negative peak; d_1). This approach allowed to take into account within the model both wave duration and amplitude. The obtained regressor was then convoluted with a standard gamma hemodynamic response function ($p = 8.6$, $q = 0.547$) and down-sampled to the BOLD time-series sampling rate (0.5 Hz, TR = 2 s). The regressor and each BOLD time-series were forced respectively to zero and the baseline value in correspondence of all artifactual and wakefulness data-segments (censored intervals). At single-subject level, beta-values of all cortical voxels were converted into z-scores calculated with respect to a null distribution obtained by re-computing the regression analysis on the same BOLD time-series after shuffling the timing of individual slow waves (intra-voxel and -subject permutations; nPerm = 1000). Importantly, the number and amplitude of slow waves was kept constant across original and shuffled regressors (i.e., relocation of slow waves within censored intervals was prevented). A group-level one-sample *t*-test was then performed at each voxel to assess statistical significance (*3dttest++*). The significance threshold was set to $q < 0.01$ after FDR correction for multiple comparisons (False Discovery Rate; Benjamini and Hochberg, 1995). A minimum, arbitrary cluster-size threshold corresponding to 50 voxels was also applied. The same analysis was repeated after the inclusion of an additional regressor in which spindles were modelled as square waves with onset-time and duration derived from the automated detection algorithm described above.

2.5. Thalamic and cerebellar involvement in sleep slow waves

Specific analyses were performed to characterize the anatomical and functional nature of thalamic and cerebellar portions recruited during the occurrence of human sleep slow waves. First, anatomical atlases were used to determine the relative distribution (percentage) of activated voxels with respect to thalamic (probabilistic atlas based on diffusion-weighted imaging; Najdenovska et al., 2018) and cerebellar (SUIT atlas; Diedrichsen et al., 2011, 2009) subdivisions. Then, thalamic and cerebellar connectivity maps were generated and used to determine the preferential functional connectivity of activated voxels with respect to the seven canonical cortical networks defined on the basis of cortical intrinsic functional connectivity (Yeo et al., 2011): visual, somatomotor, dorsal attention, ventral attention, limbic, fronto-parietal and default mode. This analysis was performed using rs-fMRI data collected during wakefulness in an independent sample of 28 subjects (see Participants section; T2*-weighted gradient-echo echoplanar sequences with 35 axial contiguous slices, TR = 2000 ms; TE = 35 ms; FA = 80°; voxel size: 3 × 3 × 4 mm; 230 vol per run). In particular, for each subject, we first computed the average BOLD-signal within 200 cortical ROIs, as defined in Schaefer et al. (2018). Then, the resting state signal from the 200 ROIs was further averaged according to the seven cortical networks, separately for each brain hemisphere (thus leading to a total of 14 large ROIs). For what concerns the thalamus, we then evaluated the partial correlation between the thalamic signal of each voxel and each homolateral cortical functional network while removing signal variance from all the left-out functional networks (Hwang et al., 2017). Regarding the cerebellum, we applied a similar procedure with two important differences. First, we measured the partial correlation between each cerebellar voxel and the contralateral cortical functional networks. Second, as described in previous work (Buckner et al., 2011), the mean

signal of neocortical voxels located in the proximity of the cerebellum (up to 6 mm) was additionally included as variable of no interest in the partial correlation procedure. This procedure ensured that the putative somatomotor region of the cerebellar anterior lobe remained relatively unaffected by the possible 'leakage' of BOLD-signal from the spatially close visual cortex. The described partial correlation procedure led to the generation of a connectivity matrix in each subject. A group-level matrix was obtained by computing the median across individual matrices. Finally, a winner-takes-all approach was applied to assign the local 'preferential connectivity' of each voxel (Hwang et al., 2017). This procedure allowed to generate functional connectivity maps of the thalamus and the cerebellum similar to those reported in Hwang et al. (2017) and Buckner et al. (2011), respectively. Then, for both the thalamus and the cerebellum, we computed the proportion of voxels connected with each of the seven networks that resulted included in the significantly activated regional clusters (see Figs. 5 and 6).

2.6. Cortical involvement in sleep slow waves

At cortical level, the sleep slow waves are known to propagate through white matter anatomical pathways between brain areas (Avvenuti et al., 2020; Massimini et al., 2004; Murphy et al., 2009). Thus, here additional analyses were performed to determine whether the specific changes in hemodynamic activity observed in association with sleep slow waves remained confined within specific cortical sites or propagated instead with some delay to other cortical areas following the spreading of electrophysiological slow waves. To this aim, we used a cross-correlation procedure to compute the similarity and relative lag of activity between different brain areas and a '*seed*' region chosen as a reference template. Specifically, the left somatomotor cortex, as defined based on the regression analysis, was here selected as *seed* region (though similar results were obtained using different *seed* areas, such as the right somatomotor cortex or the right visual cortex; *data not shown*). Then, the *seed* time-series was compared with the average BOLD-signals computed for each of the 200 ROIs of the Schaefer atlas (Schaefer et al., 2018). In particular, BOLD time-series in a time-window ranging from −4 s to +16 s with respect to slow-wave onset were first averaged across voxels belonging to each ROI, then across slow-waves and finally across subjects. The time-window of interest was selected in order to mainly include the negative portion of the hemodynamic response (Fig. 7). Such a choice was made for two reasons. First, the negative deflection is larger with respect to the slower positive deflection observed before slow-wave onset. Second, the negative deflection may be expected to more likely reflect a consequence of the neuronal silence that is associated with the *down-state* of sleep slow waves (Fultz et al., 2019). Of note, time-series included in this analysis were up-sampled to 256 Hz (linear interpolation), thus matching the EEG sampling rate, in order to improve the alignment with the timing of slow-wave onset. The cross-correlation function between the signal profile of the template and the mean time-series of each ROI was computed to estimate the relative time-lag that allowed to maximize the similarity between each pair of time-series. In addition, the magnitude of the corresponding peak in the cross-correlation function was used to evaluate the statistical significance of the similarity between examined signals. To this aim, the above-mentioned procedure was repeated following a random shuffling of the onset-timing of individual slow waves in each subject (nPerm = 1000), thus eventually obtaining a null-distribution of similarity values. ROIs for which the maximum similarity values were significantly greater than those in the null-distribution ($p < 0.05$) were used to build a propagation delay-map in which all regional lag values were re-scaled to the minimum delay-value in the map ($t = 0$ s; Fig. 8).

In order to determine whether cortical delays in hemodynamic changes may reflect the actual propagation of electrophysiological slow waves we directly compared the fMRI-based delay-map with a delay-map of EEG slow-wave propagation in source space. This map was obtained from the analysis of NREM-sleep hd-EEG recordings (256 electrodes, EGI-Philips; 500 Hz sampling frequency) obtained in a distinct set of 12 healthy adult volunteers (see Participants section). For each participant, the first 30 min of N2/N3 sleep were extracted and slow waves were automatically detected using the same algorithm described above. Then, the EEG signal was band-pass filtered between 0.5 and 4.0 Hz, and 800-ms-long data segments centered on the slow wave negative peak were extracted and source-modeled using the GeoSource 3.0 software (EGI-Philips), as described in previous work (Bernardi et al., 2019a, 2019b). In brief, a four-shell head model based on the MNI atlas and subject-specific co-registered sets of electrode positions (obtained using the Geodesic Photogrammetry System, EGI-Philips) were used to construct the forward model. The inverse matrix was computed using the standardized low-resolution brain electromagnetic tomography constraint (sLORETA; Tikhonov regularization = 10^{-2}). The source space was restricted to 2447 dipoles distributed over 7 mm^3 cortical voxels. For each slow wave, the propagation pattern was determined using an approach similar to the one described by Murphy and colleagues (Murphy et al., 2009). Specifically, for each slow wave, we defined a time-window of 100 ms centered on the timing of the maximum negative peak of the slow wave detected at scalp level. Next, for each voxel, we computed the timing of any local maxima that occurred during the time window of interest. For each voxel, after discarding secondary peaks (defined as peaks with magnitude lower that the 75% of the maximum peak across voxels), we selected the maxima that occurred most closely to the reference peak. The relative timing of these local maxima were used to create a preliminary propagation delay-map. A spatio-temporal clusterization procedure was applied with the aim of excluding potential propagation gaps (Avvenuti et al., 2020): local peaks of two spatial neighbor voxels had to be separated by less than 10 ms in order to be considered as part of the same propagation cluster. The propagation cluster including the largest signal peak was then identified and used to extract the final delay-map. The minimum observed delay, corresponding to the slow-wave origin, was set to zero. Delay-maps obtained for each wave and subject were averaged to obtain a group-level delay-map. In order to allow a comparison with the BOLD delay-map, the EEG-based delay-map was resampled to a 2 mm isovoxel resolution, matching the spatial resolution of the fMRI dataset, and mean delay values were computed for each of the 200 ROIs of the Schaefer atlas (Schaefer et al., 2018). The Pearson's correlation coefficient was eventually used to quantify the similarity between fMRI and EEG delay-maps.

2.7. Relationship between slow-wave amplitude and BOLD-signal variations

Finally, we investigated the possible relationship between the amplitude of EEG slow waves and corresponding variations in hemodynamic responses within cortical and subcortical structures. To this aim, we first performed a time-wise correlation analysis between slow wave amplitude and point-by-point (up-sampled) BOLD-signal changes for each of the significant clusters obtained from the regression analysis. In addition, a trend analysis was performed in the same areas to determine whether a relationship existed between slow wave amplitude and the delay of the regional BOLD response. Specifically, the delay of each BOLD profile was defined as the timing (relative to slow-wave onset) of the maximum positive or negative peak in subcortical and cortical regions, respectively. For this analysis, EEG slow waves were divided in three percentile classes (A_1: 0–33; A_2: 33–66; A_3: 66–100) based on their negative amplitude, and the mean delay was computed for each class. The potential trend of the mean delay as a function of EEG amplitude was then quantified with a regression analysis. Significance of the results for both the correlation and the trend analyses was tested using a within-subject permutation-based approach (nPerm = 10,000), in which the same procedures were applied after randomly shuffling the correspondence between EEG amplitudes and fMRI-derived values. Obtained p-values were separately evaluated for the positive and negative tails of the distribution, combined across subjects using the Fisher's

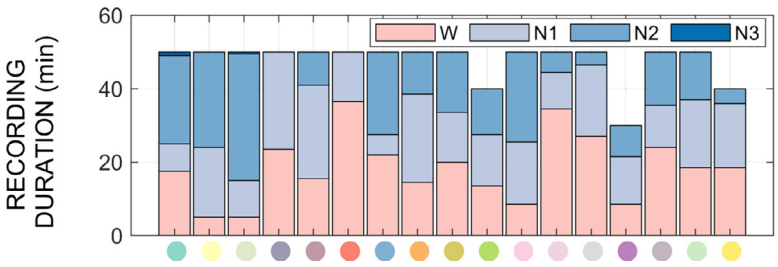

Fig. 2. Distribution of sleep stages in each participant. Each column represents a different subject. Three participants interrupted the scan session before completion of the five scheduled EEG-fMRI runs because they felt unable to fall asleep again. Overall, the EEG-fMRI data included 312.5 min of wakefulness, 266.0 min of N1, 230.0 min of N2, and 1.5 min of N3 sleep.

method (Brown, 1975) and FDR adjusted to correct for multiple comparisons.

2.8. Data availability

All relevant cortical and subcortical maps, including main results and parcellations, are available in the OSF public data repository at the following link: https://osf.io/24swv/?view_only=94179de1cdf64049b2b526789ca0f38e. Other relevant data that support the findings of this study are available from the corresponding authors on motivated request.

3. Results

3.1. Final sample and sleep macrostructure

Simultaneous EEG-fMRI recordings were performed in twenty healthy adults during an afternoon nap. However, three subjects (all males) were excluded from further evaluation as they did not reach stable sleep ($n = 1$) or presented strong artifactual activity in the EEG-signal ($n = 2$). Thus, the final sample included 17 subjects (age 28.8 ± 2.3 years, range 25–35). These participants completed three to five 10-min long EEG-fMRI runs (mean 4.7 ± 0.7), including on average 28.8 ± 9.3 min of NREM sleep (range 13.5–45.0 min; N1 = 15.7 ± 6.4 min, 58.6 ± 25.2%; N2 = 13.0 ± 10.1 min, 41.1 ± 24.8%; N3 = 0.1 ± 0.3 min, 0.2 ± 0.8%; Figs. 2, 3). A total of 1653 slow waves (97.2 ± 73.3 per participant) were automatically detected using validated algorithms (Mensen et al., 2016; Siclari et al., 2014) based on the identification of consecutive signal zero-crossings (0.25–1.0 s half-wave duration, no amplitude thresholds; see Material and Methods) and were included in subsequent analyses. Of note, none of the detected waves had a negative amplitude smaller than 10 μV, while 95% of them had an amplitude greater than 18 μV at the level of individual electrodes.

3.2. Changes in cortical and subcortical hemodynamic activity

A voxel-wise regression analysis (Fig. 1) was used to identify significant changes in brain activity associated with the occurrence of NREM slow waves. We found that slow waves were associated with two distinct blood-oxygen-level-dependent (BOLD) responses ($q < 0.01$, FDR corrected with an additional minimum cluster threshold of 50 voxels). Specifically, significant signal increases were found in subcortical structures comprising the bilateral thalamus, the cerebellum, mainly posterior portions of the brainstem, and the right caudate nucleus (Fig. 4A and Figure S1A, Table 1). Significant hemodynamic decreases were instead observed at cortical level in the bilateral somatomotor cortex, visual cortex and posterior insula, as well as in the left parahippocampal gyrus, in the right hippocampus and in the left parieto-occipital sulcus (Fig. 4B and Figure S1B, Table 1). Similar hemodynamic changes were observed for slow waves detected in N1 or N2/N3 sleep (Figure S2). Moreover, similar results were obtained by including in the analysis a regressor representing the onset-time and duration of sleep spindles (Figures S3-S8, Table S1).

An evaluation of the average temporal profile of the hemodynamic response in each significant cluster revealed that the onset of subcortical BOLD-signal increases was temporally aligned with the onset of the sleep slow wave ($t \approx 0$ s). These initial increases were followed by a slow negative BOLD-signal deflection that was especially evident in the thalamus and cerebellum. On the other hand, the strong negative signal deflection in neocortical areas was delayed by 2–4 s with respect to slow-wave onset, and was preceded by a slow, positive BOLD-signal deflection that started 4–12 s prior to slow-wave onset.

3.3. Thalamic involvement in sleep slow waves

Previous work in animal models suggested that especially centromedial thalamic nuclei may have a key role in the modulation of sleep slow waves (Gent et al., 2018b). In order to investigate whether this may be true also in humans, here we analyzed and characterized the anatomical and functional nature of thalamic portions recruited during the occurrence of human sleep slow waves (Fig. 5). First, we determined the percentage of activated voxels that fell within specific thalamic substructures identified using a probabilistic atlas of the human thalamus based on diffusion-weighted imaging (Najdenovska et al., 2018). For both the left and the right thalamus, we found that significant BOLD-signal changes especially involved medial nuclei located anteriorly, centrally and posteriorly (Figs. 5D-E). In particular, activated portions of the thalamus included ~40% of anterior thalamic nuclei (A), ~30% of posterior nuclei (medial pulvinar, PuM; central lateral nucleus, CL; lateral posterior nucleus, LP), ~20% of ventral anterior nuclei (VA) and ~18% of mediodorsal nuclei (MD). Of note, however, the inclusion of sleep spindles in a regressor of no interest led to the almost complete disappearance of the anterior thalamic portion, suggesting that recruitment of anterior nuclei may be actually related to the occurrence of spindles (Figure S6).

Second, we evaluated the functional organization of activated thalamic portions by determining the preferential functional connectivity of each voxel with each of the seven main canonical brain networks (Hwang et al., 2017; Yeo et al., 2011): visual, somatomotor, dorsal attention, ventral attention, limbic, fronto-parietal and default mode (Fig. 5A-B). We found that the portion of thalamus recruited during sleep slow waves was especially connected with areas of the limbic system (Fig. 5C). Indeed, the activated thalamic cluster included ~70% of all thalamic voxels showing a preferential connectivity with this particular network. Other represented networks included the default mode network (~22%) and the frontoparietal network (~20%).

3.4. Cerebellar involvement in sleep slow waves

Changes in cerebellar activity have been previously reported as a function of sleep stage as well as in association with the occurrence of sleep slow waves (for a detailed review see Canto et al., 2017). Yet, the determinants of sleep-dependent changes in cerebellar activity and the possible role of the cerebellum in sleep regulation are still largely unknown. In order to advance current knowledge on these key aspects, here we performed a detailed evaluation of cerebellar activity related to the occurrence of NREM slow waves (Fig. 6). As described above for the thalamus, we first determined the percentage of activated voxels that fell within specific cerebellar areas identified using the SUIT anatomical atlas (Diedrichsen et al., 2011, 2009). The results of this analysis are

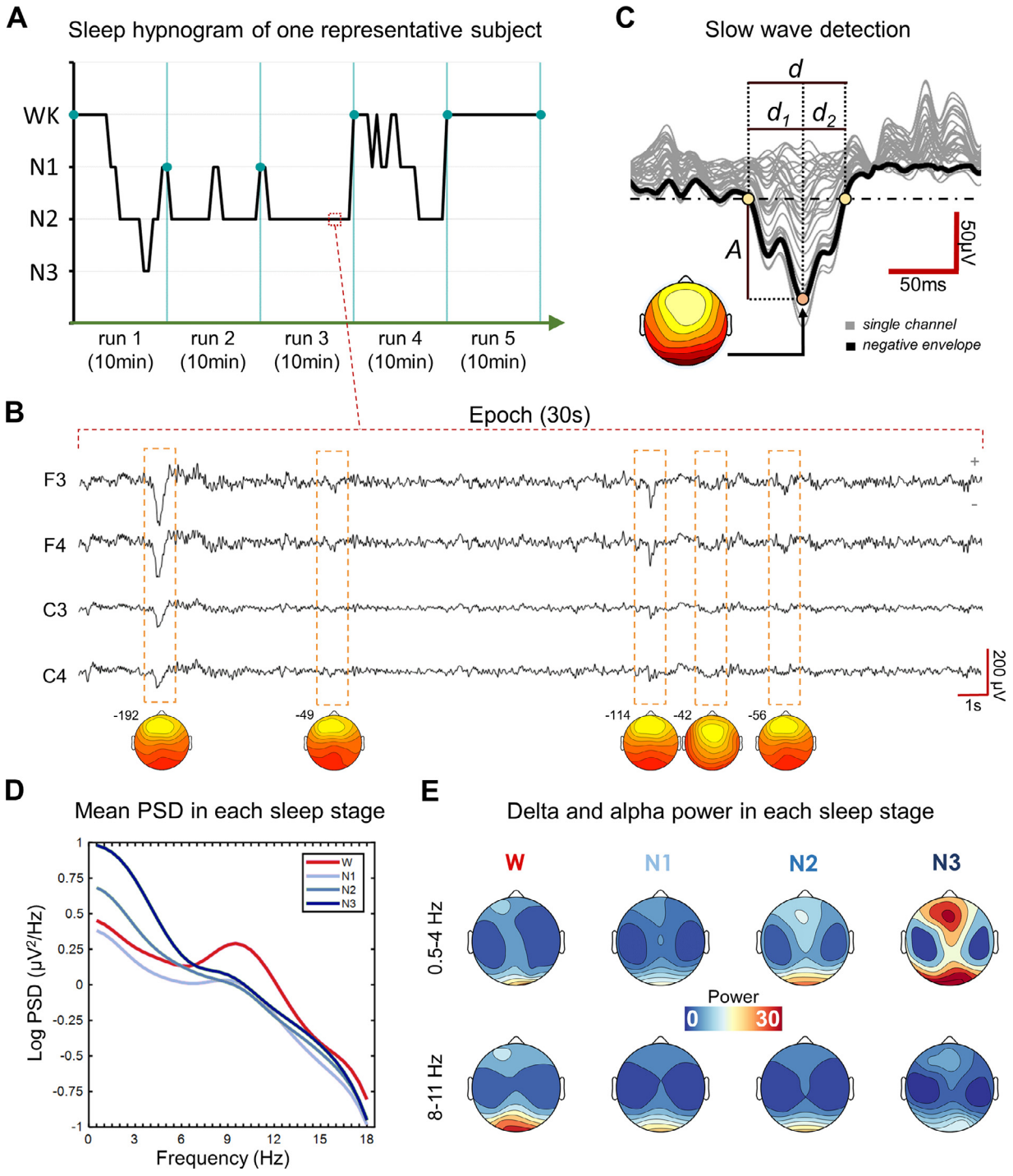

Fig. 3. Scoring and analysis of EEG recordings. (A) Sleep hypnogram of one study participant. Vertical lines mark the end of EEG-fMRI acquisition runs. (B) EEG traces of a N2 epoch of the same participant shown in panel A. Orange dashed boxes mark detected slow waves. The topographic distributions of the slow waves are shown below the respective boxes (here yellow indicates more negative values), together with the maximum negative amplitude observed across all electrodes (in μV). In each plot, the color-scale is set to range between the minimum and maximum signal-amplitude values. (C) Schematic representation of the approach used to detect and characterize sleep slow waves. Negative half-waves were automatically detected through the identification of negative peaks comprised between consecutive signal zero-crossings. *A* = amplitude; *d* = half-wave duration; d1 = time from first zero-cross to negative peak; d2= time from negative peak to second zero-cross. (D) Mean power spectral densities (PSD) obtained across all studied volunteers for wakefulness (W), N1, N2, and N3 sleep. PSD values were computed in two frontal (F3, F4) and two central (C3, C4) electrodes and then averaged. (E) Changes in delta and alpha power across sleep stages were evaluated to verify the accuracy of sleep scoring procedures. As expected, all sleep stages are characterized by a reduction in alpha activity (8–11 Hz) with respect to wakefulness, while delta activity (0.5–4 Hz) increases from N1 to N3 sleep. (For interpretation of the references to color in this figure legend, the reader is referred to the web version of this article.)

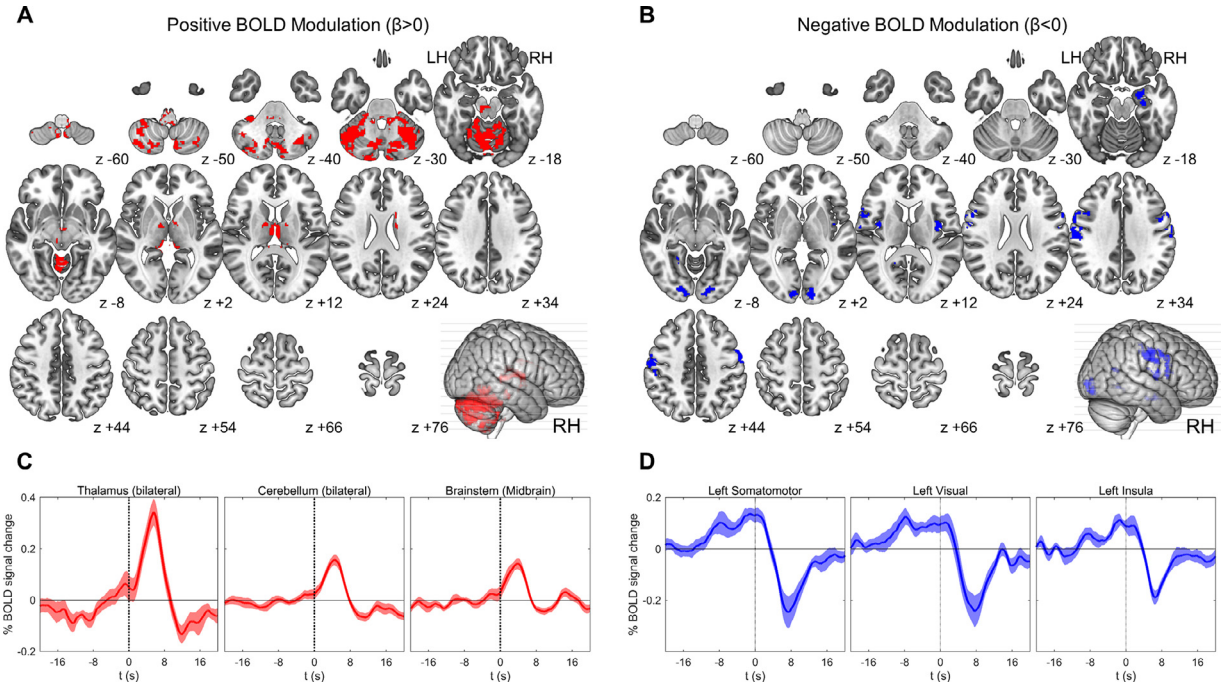

Fig. 4. Results of the regression analysis. (A-B) Brain structures associated with a significant ($q < 0.01$, cluster size ≥ 50 voxels) BOLD-signal (A) increase (red) or (B) decrease (blue). Brain images were generated using MRIcron (https://www.nitrc.org/projects/mricron). (C-D) Mean BOLD-signals (up-sampled to the EEG sampling rate) and relative standard errors for three subcortical (C) and three cortical (D) of the identified significant clusters. Time $t = 0$ s corresponds to slow-wave onset. (For interpretation of the references to color in this figure legend, the reader is referred to the web version of this article.)

Table 1
Results of regression analysis. Brain areas showing a significant BOLD-signal increase (positive) or decrease (negative) in relation to the occurrence of sleep slow waves ($q < 0.01$, cluster size ≥ 50 voxels). The table includes the number of voxels and the coordinates of the center of mass of each significant cluster in standard MNI space.

Signal change	Region	Voxels	CM x	CM y	CM z
Positive	Brainstem (Medulla)	120	−0.8	−38.5	−46.7
	Brainstem (Midbrain)	95	−7.3	−25.3	−15.7
	Caudate Nucleus	76	+17.9	−0.8	+25.5
	Cerebellum	6322	−5.2	−62.7	−29.2
	Cerebellar Tonsil	121	−2.4	−54.7	−61.3
	Medial Thalamus	734	+1.0	−19.0	+7.6
Negative	Left Posterior Insula	64	−39.0	−4.8	+10.2
	Right Posterior Insula	123	+37.9	−5.3	+12.1
	Right Hippocampus	135	+24.8	−10.1	−18.9
	Left Parahippocampus	50	−22.0	−54.6	−4.9
	Letf Parieto-Occipital Sulcus	64	−17.0	−58.6	+17.5
	Left Somatomotor Cortex	800	−57.4	−7.4	+32.5
	Right Somatomotor Cortex	279	+58.4	−2.1	+34.5
	Left Visual Cortex	176	−15.5	−90.5	−5.7
	Right Visual Cortex	268	+13.5	−90.8	−3.5

presented in Fig. 6C-D and indicate a broad involvement of the vermis and of the superior portions of both cerebellar hemispheres. Then, we evaluated the functional relationship between activated cerebellar portions and the seven canonical brain networks (Fig. 6A-B). We found that the fractions of cerebellum involved in sleep slow waves were especially connected with areas of the somatomotor network. In fact, the activated cluster included ~45% of all cerebellar voxels showing a preferential connectivity with this particular network. Other represented networks included the frontoparietal network (~34%) and the ventral attention network (~28%).

3.5. Cortical involvement in sleep slow waves

Macro-scale hd-EEG studies in humans showed that slow waves are not stationary events, but instead propagate at cortical level through anatomically connected pathways (Avvenuti et al., 2020; Massimini et al., 2004; Murphy et al., 2009). This propagation of electrophysiological slow waves may determine a relative variability in the timing of hemodynamic changes across cortical regions. Of note, BOLD-changes occurring ahead or delayed with respect to the actual onset of slow waves could be missed by conventional fMRI analyses (Mitra et al., 2015). In line with this possibility, a preliminary evaluation of the mean BOLD-signal time-courses within areas of the seven canonical networks showed similar patterns of changes in all regions, thus suggesting that most cortical areas may actually present some degree of modulation in association with the occurrence of sleep slow waves (Fig. 7).

In light of these observations, further analyses were performed to investigate whether hemodynamic cortical changes showed a relative propagation similar to the one described for electrophysiological slow waves. Specifically, we first computed the average BOLD-signal across

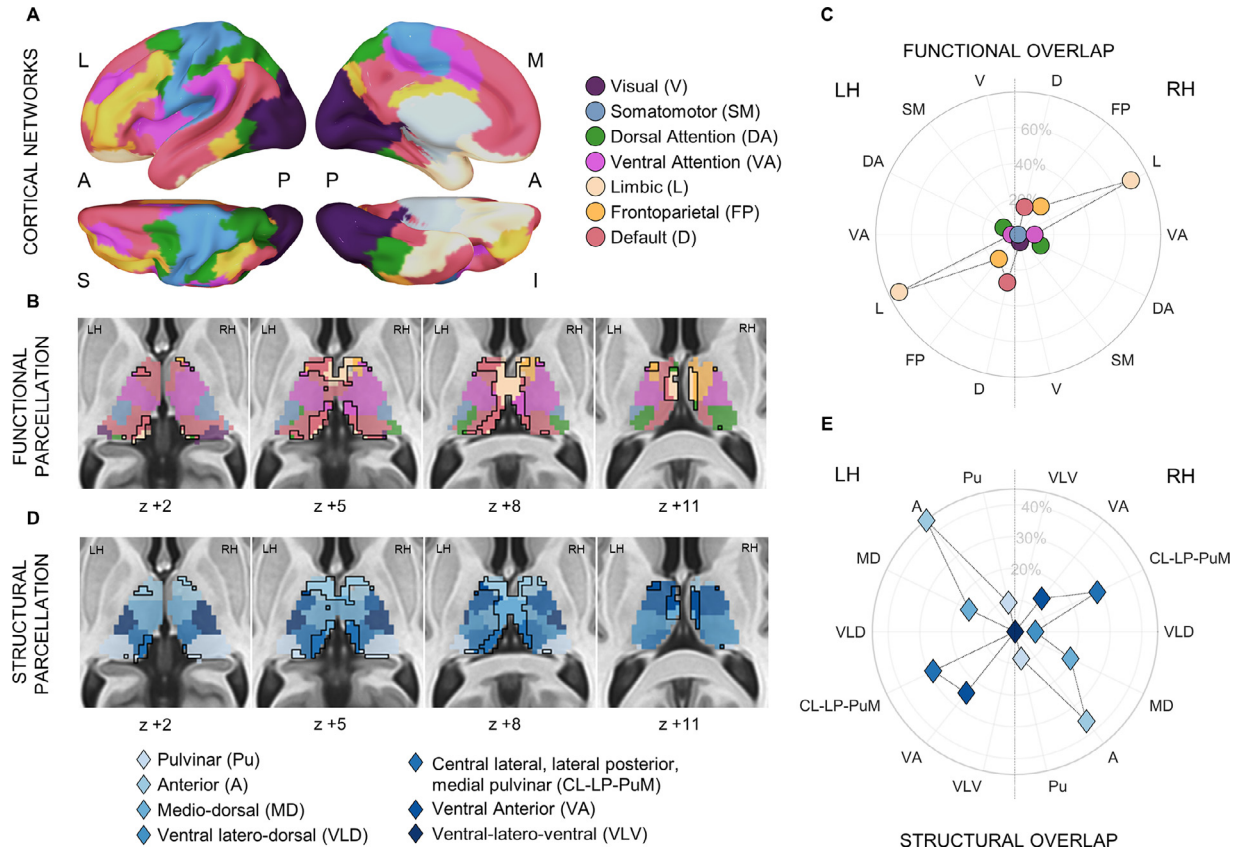

Fig. 5. Thalamic involvement in sleep slow waves. (A) The seven canonical networks used to determine the preferential connectivity of each thalamic voxel. (B) Parcellation of the thalamus based on the preferential functional connectivity of each voxel. (C) Radial plot showing the proportions of activated voxels having a preferential connectivity with each of the seven canonical networks with respect to the totality of thalamic voxels. (D) Parcellation of the thalamus based on the Najdenovska atlas. (E) Radial plot showing the proportions of activated voxels attributed to each anatomical area with respect to the totality of thalamic voxels. In (B) and (D), the portion of the thalamus activated in association with the occurrence of sleep slow waves ($q < 0.01$, cluster size ≥ 50 voxels) is highlighted and enclosed with a black line.

slow waves and subjects within 200 cortical regions of interest (ROIs) of the Schaefer functional atlas (Schaefer et al., 2018; Fig. 7B-C shows the relative amplitude of positive and negative BOLD-signal peaks for all ROIs). Then, a cross-correlation analysis was performed between a seed time-series corresponding to the left somatomotor cortex and the time-series of all brain ROIs. This investigation confirmed that most brain areas showed similar slow-wave-dependent hemodynamic changes, which however occurred at different delays in distinct brain regions (Fig. 8; also see Figure S9). In particular, the lowest delays were found in areas encompassing the somatomotor cortex, the premotor-prefrontal cortex and the anterior insula, while the highest delays were found in the inferior and lateral occipital and temporal cortex. These observations were substantially confirmed through a network-level analysis based on seven large bilateral ROIs. In fact, the lowest latency was found in the somatomotor network, followed by the ventral attention (+ 0.08 ± 0.08 s, mean ± standard error computed across areas of the same network) and the dorsal attention (+ 0.33 ± 0.19 s) networks. The highest delays were instead found in the visual (+ 0.81 ± 0.18 s) and limbic (+ 1.01 ± 0.39 s) networks.

Interestingly, while spanning a much broader time-frame (in the order of seconds vs. tens to few hundred of milliseconds), the fMRI delay-map was strikingly reminiscent of the one obtained from the analysis of slow-wave propagation in source-level hd-EEG data (Murphy et al., 2009). In order to allow a direct comparison between the hemodynamic and the electrophysiological delay-maps, here we re-analyzed NREM-sleep hd-EEG recordings (256 electrodes, EGI-Philips; 500 Hz sampling frequency) obtained in a distinct set of 12 healthy adult volunteers (see Materials and Methods). In particular, slow waves were automatically detected in the first 30 min of N2/N3 sleep, and their regional propagation delays were computed in source space using a previously described approach (Murphy et al., 2009; Siclari et al., 2014). In line with results obtained for hemodynamic changes, electrophysiological slow waves showed the lowest latency in areas encompassing somatomotor cortex, insula and premotor areas, while the highest delay was observed in temporal and occipital regions. A correlation analysis at ROI-level ($N = 182$) confirmed the existence of a significant association between hemodynamic and electrophysiological delay-maps (Pearson's $\rho = 0.264$; $p = 0.0003$; Figure S10). The same analysis performed at network-level ($N = 7$) also yielded a strong correlation with $\rho = 0.893$ ($p = 0.007$; Fig. 8C), suggesting that the relatively modest correlation coefficient obtained at ROI-level could be in part ascribed to inaccuracies in source estimation.

3.6. Relationship between slow-wave amplitude and BOLD-signal variations

Finally, we investigated whether variations in the properties of electrophysiological slow waves corresponded to variations in the profiles of regional hemodynamic responses. A correlation analysis between slow wave amplitude and point-by-point BOLD-signal changes revealed a significant positive relationship between EEG amplitude and the absolute magnitude of the observed positive subcortical and the negative cortical signal-deflections ($q < 0.01$; Fig. 9A-B and Figures S11, S12). Consistent with this, we also observed a significant correlation between the maximum amplitude of the positive BOLD-signal change in subcortical structures and the maximum negative signal change in cortical areas ($q < 0.001$; Figure S13). Of note, the small positive BOLD-signal deflection

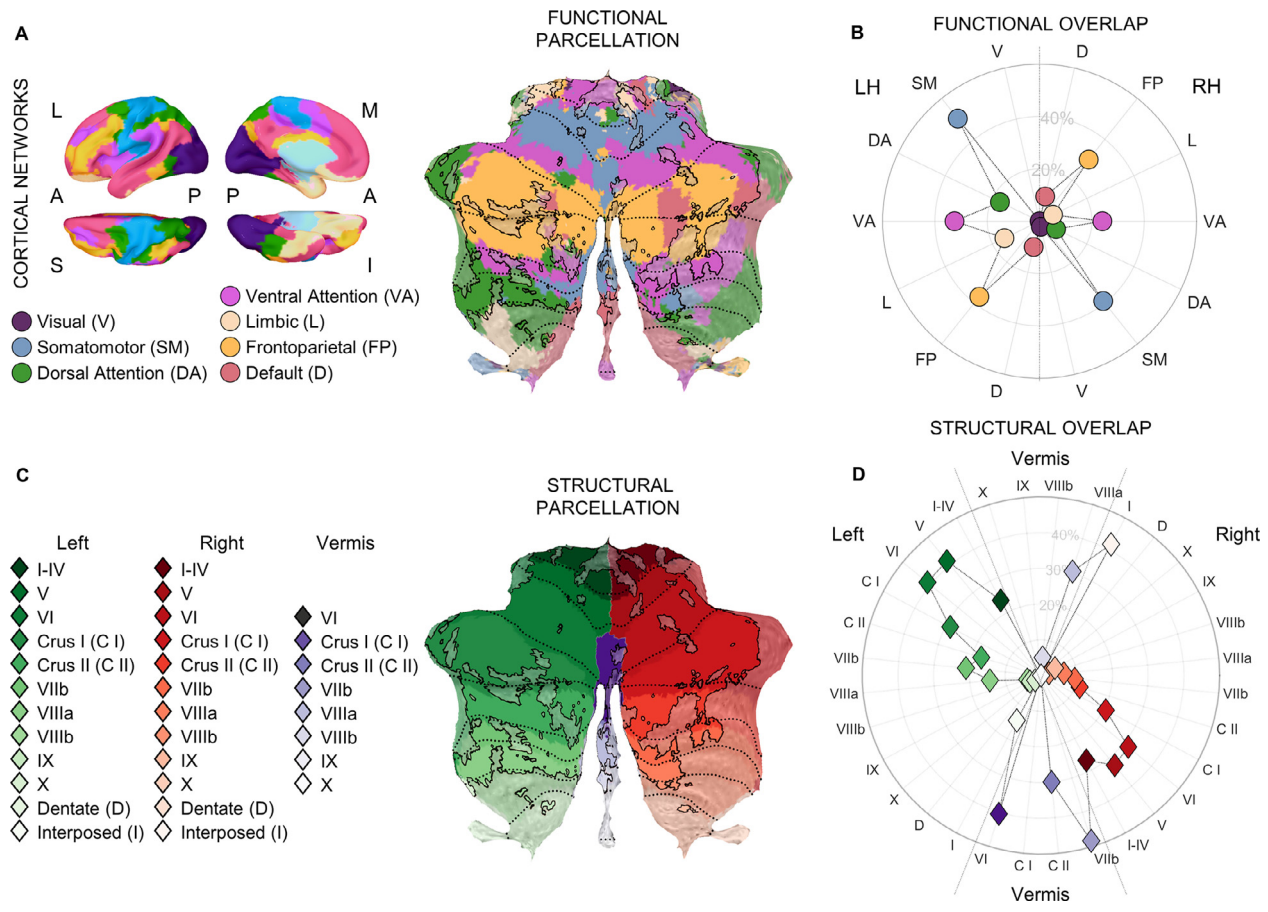

Fig. 6. Cerebellar involvement in sleep slow waves. (A) The seven canonical networks and the correspondent parcellation of the cerebellum based on the preferential connectivity of each voxel. (B) Radial plot showing the proportions of activated voxels having a preferential connectivity with each of the seven canonical networks with respect to the totality of cerebellar voxels. C) Anatomical parcellation of the cerebellum based on the SUIT anatomical atlas. (D) Radial plot showing the proportions of activated voxels attributed to each anatomical area with respect to the totality of cerebellar voxels. In (A) and (C), the portion of the cerebellum activated in association with the occurrence of sleep slow waves ($q < 0.01$, cluster size ≥ 50 voxels) is highlighted and enclosed with a black line.

observed in cortical areas immediately before or around slow-wave onset, and the late negative component observed in subcortical structures were also significantly modulated by slow wave amplitude. Interestingly, significant positive correlations were found up to 4 s before slow-wave onset in thalamus, somatomotor cortex, insula and hippocampus (Figure S11), in line with previous evidence indicating a possible central role of these regions in slow wave generation (Murphy et al., 2009). The evaluation of hemodynamic changes for distinct slow-wave amplitude percentile classes (A_1: 0–33; A_2: 33–66; A_3: 66–100) confirmed that larger slow waves were associated with larger BOLD-signal changes (also see Figure S14, which shows BOLD-signal changes associated with slow waves classified as small or large based on a fixed negative amplitude threshold corresponding to 40 μV), and also revealed a relative modulation of the latency of such changes (trend analysis, $p < 0.01$; Fig. 9C and Figure S12). In fact, larger slow waves were associated with larger hemodynamic variations that occurred earlier in time, while smaller slow waves were associated with smaller hemodynamic changes that tended to be shallower and to peak later in time.

4. Discussion

The present study provided an in-depth spatio-temporal characterization of cortical and subcortical hemodynamic changes associated with sleep slow waves in humans. Our results can be summarized in four main findings. First, we showed that sleep slow waves are associated with significant BOLD-signal increases in subcortical structures, including the brainstem, thalamus and cerebellum, whereas in cortical areas a slow BOLD-signal increase precedes slow-wave onset and is followed by a prominent decrease. Second, we showed that positive subcortical changes occur within specific portions of thalamus and cerebellum, including medial thalamic nuclei having a strong connectivity with bilateral limbic functional networks, and cerebellar areas having a preferential connectivity with the somatomotor network. Third, we showed that cortical hemodynamic responses occur at different delays across a broad extent of the cortical mantle, with the shortest delay observed in somatomotor areas and the highest delay in temporal and lateral occipital areas. Importantly, the BOLD-signal propagation pattern substantially mirrors the spreading of electrophysiological slow waves. Finally, by investigating the relationship between EEG slow waves and hemodynamic activity, we found that slow-wave amplitude is directly correlated to the magnitude and the latency of the hemodynamic BOLD-signal changes in both cortical and subcortical areas. Overall, these findings indicate that human slow waves are associated with a complex chain of interactions among subcortical and cortical brain structures, in line with evidence obtained in animal models.

4.1. Sleep slow waves are associated with hemodynamic changes in brainstem and thalamus

Our results indicate that human sleep slow waves are associated with hemodynamic changes in the brainstem and the thalamus, including an initial signal increase followed by a late, less pronounced negative deflection. Of note, the thalamic activation especially involves midline nuclei presenting a strong connectivity with the limbic network

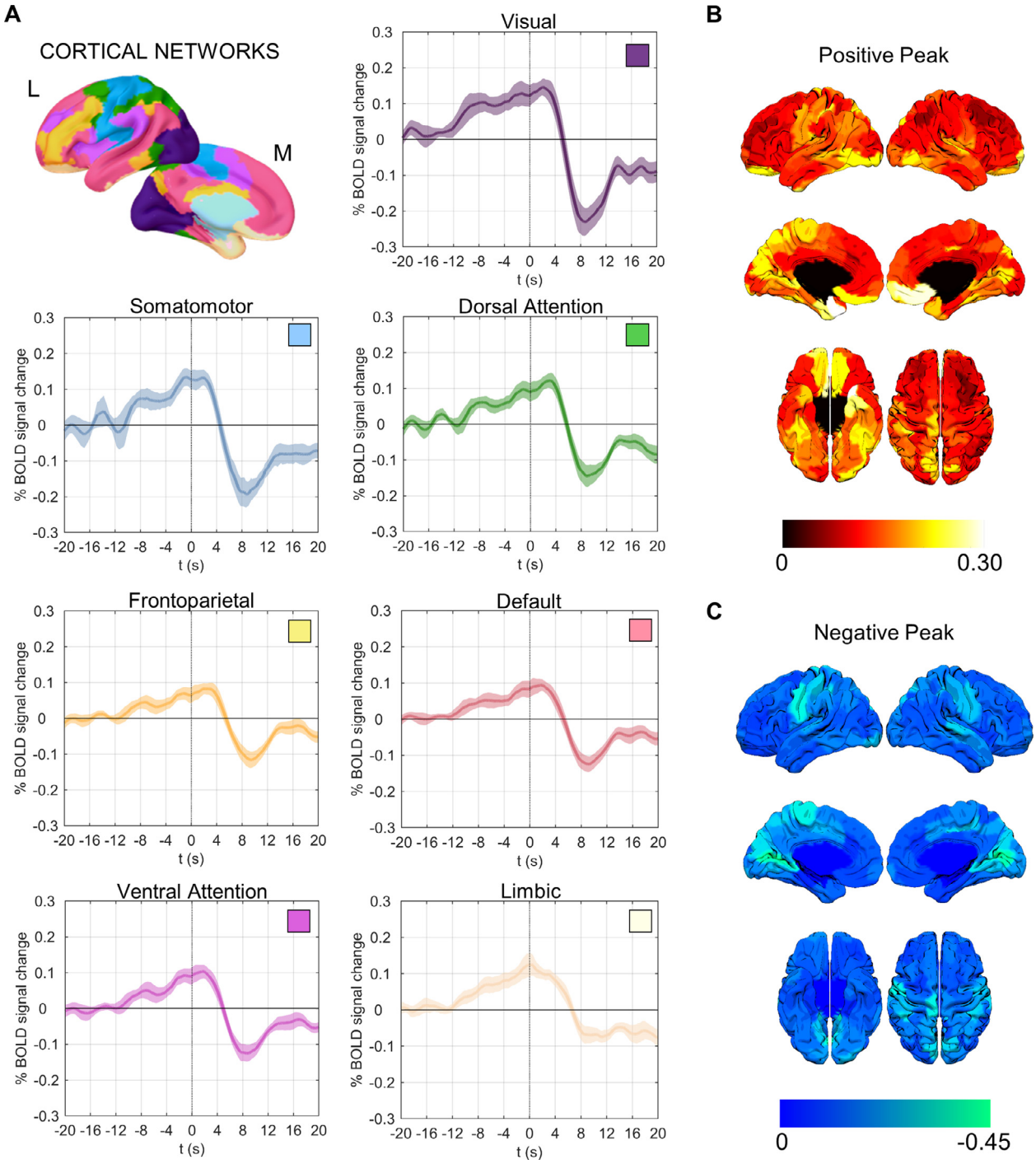

Fig. 7. Slow-wave-related hemodynamic changes across the cortical mantle. (A) Mean BOLD-signal time-courses (± standard error) associated with sleep slow waves in the seven canonical networks. Time $t = 0$ s corresponds to slow-wave onset (positive-to-negative zero crossing). Amplitude of the positive (B) and negative (C) peaks in each of the 200 ROIs of the Schaefer atlas. Brain surface plots were generated using the Surf Ice software (https://www.nitrc.org/projects/surfice/). The largest negative amplitudes were found in primary cortices, while the largest positive amplitudes were also found in areas of the limbic network.

- the so-called 'limbic thalamus' (Colavito et al., 2015; Vertes et al., 2015). At the brainstem level, two main clusters of activation were found in the posterior midbrain and medulla. The posterior brainstem contains the *reticular formation* (Brown et al., 2012; Moruzzi and Magoun, 1949), which is known to send projections to the thalamic reticular nucleus and the midline and intralaminar thalamic nuclei (Mountcastle and Poggio, 1974; Steriade and Glenn, 1982). This may explain the co-activation of these structures in association with sleep slow waves.

The involvement of brainstem and medial thalamus in human slow waves is consistent with previous findings in animal models (Gent et al., 2018a; Neske, 2016). Indeed, while the *slow oscillation* underlying the generation of sleep slow waves is traditionally regarded as a prominently cortical phenomenon due to its persistence after thalamic lesion (Steriade et al., 1993b) and in deafferented cortical slabs (Timofeev et al., 2000), accumulating evidence indicates a direct involvement of the brainstem and the thalamus in modulating important properties of NREM slow waves. In particular, these structures have been

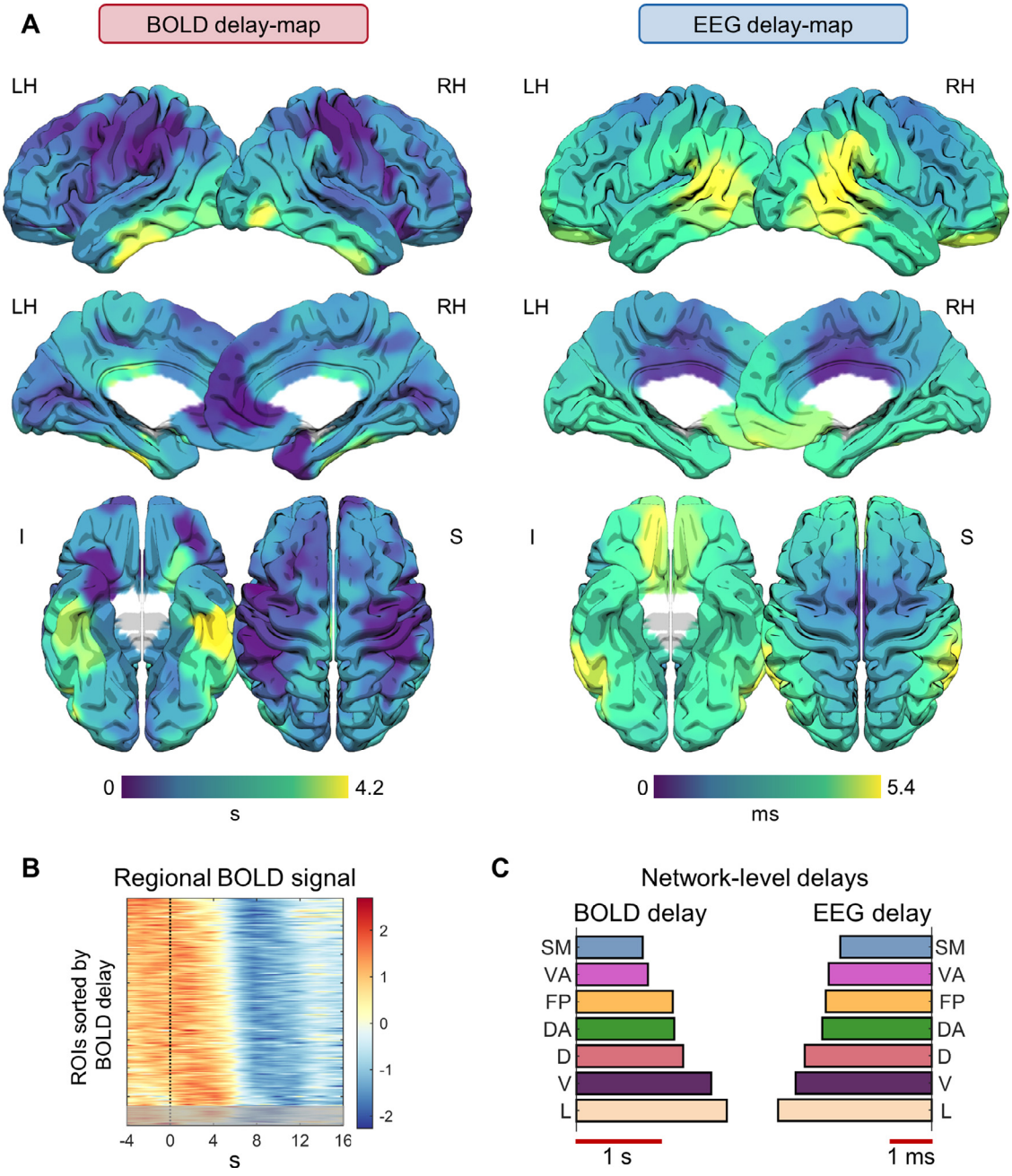

Fig. 8. Hemodynamic and electrophysiological signal propagation during sleep slow waves. (A) Mean cortical delay-maps. Brain surface plots were generated using the Surf Ice software (https://www.nitrc.org/projects/surfice/). Here the yellow color indicates a high delay, while the dark-blue color indicates a low delay. All the 200 ROIs of the Schaefer atlas are shown. It is important to note that these maps reflect a mean propagation pattern, which may not correspond to the propagation pattern of each individual slow wave. (B) Mean hemodynamic brain activity changes (z-score) in the 200 ROIs, sorted according to relative delay values. ROIs characterized by a non-significant cross-correlation with the seed region were put in the bottom section of the image and are covered by a gray shadow. (C) Mean propagation delays computed for the seven (bilateral) canonical networks for BOLD (left) and EEG (right) signals. SM: somatomotor, VA: ventral attention, FP: fronto-parietal, DA: dorsal attention, D: default mode, V: visual, L: limbic. (For interpretation of the references to color in this figure legend, the reader is referred to the web version of this article.)

suggested to play a fundamental role in triggering and synchronizing the *up-state* at each cycle of the *slow oscillation* (Amzica and Steriade, 1995; Contreras and Steriade, 1995; Eschenko et al., 2012; Mena-segovia et al., 2008; Schweimer et al., 2011). Consistent with this view, previous work showed that cortical *up-states* are preceded by spontaneous thalamic spikes (Gent et al., 2018a; Sheroziya and Timofeev, 2014; Slézia et al., 2011; Ushimaru and Kawaguchi, 2015) and may be induced through electrical or optogenetic stimulation of the thalamus (David et al., 2013; Gent et al., 2018a; Honjoh et al., 2018; Poulet et al., 2012). Moreover, thalamic deafferentation of the cortex leads to a significant reduction in the frequency of *slow oscillations* (David et al., 2013; Lemieux et al., 2014). On the same line, the noradrenergic locus coeruleus, which was likely among the activated brainstem portions in the present study, has been shown to increase its firing during *down-to-up state* transitions (Eschenko et al., 2012). Our results support the possibility of a similar regulating role of subcortical structures during human slow waves. Moreover, the specific recruitment of limbic-related thalamic portions is congruous with evidence indicating a key-role of NREM slow waves

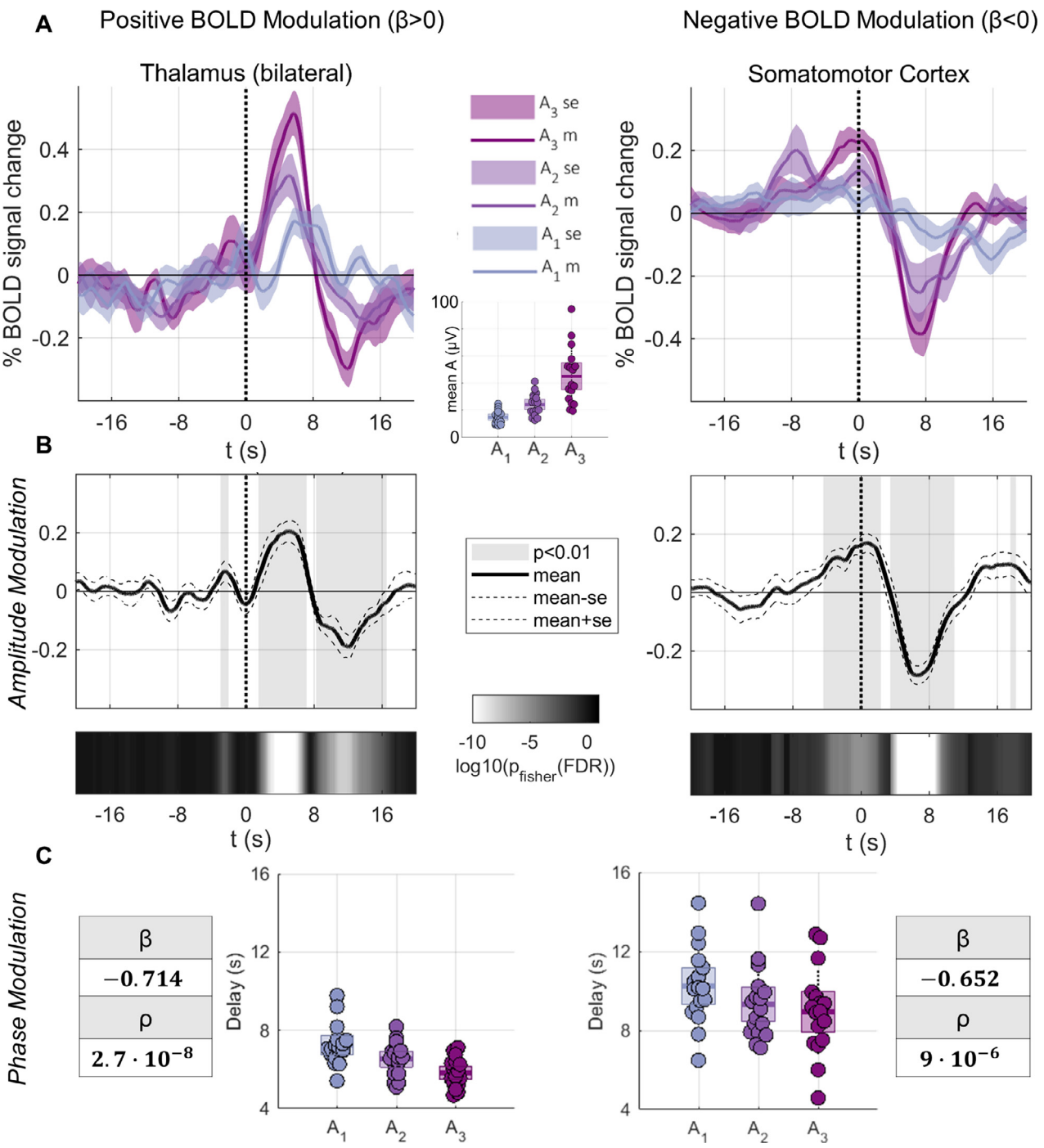

Fig. 9. Relationship between EEG slow-wave properties and regional hemodynamic changes. (A) Temporal evolution of BOLD-signals (averaged across subjects), for three classes of slow waves defined based on amplitude percentiles (A1: 0–33; A2: 33–66; A3: 66–100). (B) Point-by-point correlation between slow-wave amplitude and BOLD-signal change for representative subcortical (thalamus) and cortical (somatomotor cortex) structures. The gray shadowed areas indicate significant effects with $q<0.01$. (C) Relative delays of the positive (for thalamus) and the negative (for somatomotor cortex) BOLD-signal peaks for each of the three wave classes. A regression was performed to determine whether a relationship existed between slow wave amplitude and the relative latency of hemodynamic peaks. Correspondent beta and p-values are reported in the gray boxes.

in learning and memory consolidation (Diekelmann and Born, 2010; Miyamoto et al., 2017; Tononi and Cirelli, 2014).

4.2. Cerebellar involvement in human sleep slow waves

A mainly positive hemodynamic modulation similar to the ones found in the brainstem and the thalamus was also observed in the cerebellum. In fact, an association between sleep slow waves and cerebellar activity has been previously described both in animal models (Roš et al., 2009; Steriade et al., 1971a, 1971b) and in humans (Dang-Vu et al., 2008). In addition, during N2 sleep, changes in cerebellar activity have been found to accompany the occurrence of K-complexes (Jahnke et al., 2012). Evidence obtained in ketamine-anesthetized rats suggests that the neocortex may entrain the cerebellum during the alternation of *down-* and *up-states* (Rowland et al., 2010), while the cerebellum may in turn have a relevant role in the fine-tuning of cortical slow waves

(Canto et al., 2017). Nevertheless, the mechanism and functional meaning of cerebellar recruitment during cortical *slow oscillations* is still to be fully understood. One intriguing possibility is that changes in cerebellar activity play a role in the consolidation of motor memories, and possibly of other cognitive skills (Canto et al., 2017). In line with this view, here we found that portions of the cerebellum activated during sleep slow waves especially include those connected with the somatomotor network and, to a lesser extent, to the spatially close frontoparietal and ventral-attention networks.

4.3. Human slow waves are coupled with cortically propagating hemodynamic waves

At the cortical level, we found that slow-wave onset is associated with a negative BOLD-signal deflection that could reflect the occurrence of locally synchronized *down-states* characterized by neuronal silence. In particular, we observed significant cortical clusters displaying large BOLD-signal decreases in bilateral insula, somatomotor cortex and visual cortex, as well as in the right hippocampus, left parahippocampus and left parieto-occipital sulcus. However, similar hemodynamic changes were also found to occur at different delays across distinct brain areas, covering a broad extent of the cortical mantle. In fact, we found that the insula, somatomotor and premotor regions were among the areas with the lowest relative delay, while the highest delays were found in the occipital and temporal cortex. This finding is consistent with the known cortical propagation of electrophysiological slow waves. Indeed, previous work showed that most EEG slow waves have a well-defined and circumscribed origin that more often involve centrofrontal brain areas likely including the somatomotor cortex and the insula (Avvenuti et al., 2020; Massimini et al., 2004; Menicucci et al., 2009; Murphy et al., 2009), from which they propagate toward more anterior and posterior areas. In line with this, here we showed that the regional delays of hemodynamic changes significantly correlate with the propagation delays of electrophysiological slow waves, thus implying a direct coupling between the two phenomena. This finding is especially interesting in light of recent evidence linking EEG slow waves, hemodynamic changes and CSF movements (Fultz et al., 2019). Indeed, while CSF movement was not directly assessed in the present work, our results suggest that slow-wave propagation could generate a hemodynamic gradient that may ultimately favor CSF flow and the clearance of metabolic wastes. Interestingly, this mechanism could also contribute to explain the recent observation of a direct relationship between slow wave activity (1–4 Hz delta power) and glymphatic CSF movement (Hablitz et al., 2019). Indeed, here we found that the amplitude of electrophysiological slow waves is positively related to the magnitude and inversely related to the delay of cortical (and subcortical) BOLD-signal changes. Thus, larger slow waves are associated with stronger and faster hemodynamic changes that may lead to a more efficient mobilization of the CSF. This hypothesis would be consistent with previous reports of a direct link between alterations of slow wave activity and cognitive decline related to the accumulation of β-amyloid in the medial prefrontal cortex of older individuals (De Gennaro et al., 2017; Mander et al., 2015).

Why slow waves show the lowest delay, and thus, a more common origin, in insula and somatomotor and premotor cortex, is unclear. These regions are characterized by a strong noradrenergic innervation (Gaspar et al., 1989; Javoy-Agid et al., 1989; Lewis and Morrison, 1989) and may thus be particularly affected by the overall reduction of activating neuromodulators from wakefulness to NREM sleep. Moreover, the same areas also seem to represent a preferential origin for large and widespread slow waves (including K-complexes), whose generation/synchronization mechanism has been suggested to depend on phasic activity of ascending activating systems (Bernardi et al., 2018; Siclari et al., 2014). Another intriguing possibility is that the spatial distribution of slow-wave origin reflects a role of slow waves in the maintenance of sensory and motor disconnection during sleep (Funk et al., 2016). Possibly consistent with this interpretation, we found that the cortical negative signal deflection is preceded by a slow rise of the BOLD-signal, which peaks around the timing of slow wave onset. This BOLD-signal increase may reflect spontaneous or stimulus-induced increases in cortical activity that eventually trigger a response-suppression represented by the sleep slow wave. In fact, a similar mechanism has been suggested to subserve the sleep-protective function of stimulus-induced K-complexes (Andrillon and Kouider, 2020; Laurino et al., 2019, 2014; Riedner et al., 2011).

4.4. Limitations

Present analyses were performed on EEG-fMRI data collected during an afternoon nap and most participants failed to reach deep, N3 sleep. It should be noted, however, that the relative sparsity of slow waves occurring in light sleep can be expected to minimize potential confounds related to the overlap of hemodynamic responses associated with slow waves occurring in close temporal sequence. This is especially important given the slow temporal evolution of the hemodynamic response and its relative propagation at cortical level. Given these considerations, future studies should verify whether trains of large slow waves that occur in N3 may involve partially distinct sets of brain regions or be associated with different response patterns (though preliminary analyses suggest that similar hemodynamic changes may be associated with slow waves occurring in isolation or in temporal vicinity with other slow waves, at least in light sleep; Figure S15). Moreover, there is evidence for the existence of different subtypes of slow waves, including widespread waves such as K-complexes (*type I* slow waves) and more local (*type II*) slow waves, which co-exist during NREM sleep and likely rely on different synchronization mechanisms (Bernardi et al., 2018; Siclari et al., 2014). It is therefore unlikely that all slow waves engage the whole set of brain regions in an identical manner. Indeed, not only each individual slow wave may recruit partially different areas depending on its specific origin and propagation pattern, but the same areas could be also engaged differently by distinct slow-wave subtypes.

Importantly, the use of an afternoon nap and of a sleep restriction protocol introduced homeostatic and circadian differences with respect to previous work on the hemodynamic correlates of sleep slow waves, and especially the study by Dang-Vu and colleagues (Dang-Vu et al., 2008; but see Caporro et al., 2012). Circadian and homeostatic factors are known to affect slow wave parameters such as incidence and amplitude (e.g., Riedner et al., 2007), but are commonly assumed to not affect the mechanisms involved in slow wave generation or propagation, nor their relationship with BOLD-signal changes. Nevertheless, differences in the experimental approach may contribute to explain the inconsistent findings between present and previous studies and should be addressed by future investigations.

Recent work suggested that K-complexes, changes in sub-cortical arousals and episodic variations of peripheral indices reflecting sympathetic activity could be associated with widespread, non-specific fMRI-signal changes at cortical level (Duyn et al., 2020; Özbay et al., 2019). However, control analyses showed that autonomic dynamics alone, as measured through changes in heart-rate (Chang et al., 2009), cannot explain the observed changes in cortical BOLD-signals associated with slow waves (Figures S16 and S17). In fact, a non-specific, widespread BOLD-signal variation seems unable to explain our present observations for several additional reasons. First, we found similar changes in hemodynamic activity for both large slow waves, potentially including K-complexes, and small slow waves, which do not display a clear association with arousal-related indices (Bernardi et al., 2018; Halász, 2016; Siclari et al., 2018). Second, hemodynamic changes were found to present relevant regional differences in terms of both amplitude and latency relative to slow wave onset, while a non-specific generalized response would have been expected to similarly affect most cortical areas. Finally, we found that regional delays of slow-wave propagation in EEG significantly correlate with BOLD-signal delays, thus implying a common neural basis. This correlation appears not to be driven by

artifactual or vascular signal components (Erdoğan et al., 2016; Figure S18). Nevertheless, it will be important for future studies to investigate whether phasic changes in autonomic activity may affect the cortical and subcortical expression of sleep slow waves.

Finally, we note that, in contrast with the definition proposed in the AASM manual for sleep scoring (Iber et al., 2007), here we defined as slow waves all negative half-waves in the 0.5–2 Hz frequency range, regardless of their negative or peak-to-peak amplitude. This choice, shared with numerous previous investigations (e.g., Avvenuti et al., 2020; Bernardi et al., 2019a; Riedner et al., 2007; Siclari et al., 2018), has several justifications the detailed description of which lies beyond the scope of the present study. In brief, while useful for standardizing sleep scoring and for the analysis of sleep macro-architecture, the classical 75 μV peak-to-peak amplitude threshold does not have an actual physiological justification. This is especially true given that slow-wave amplitude has been shown to change considerably both across and within individuals (for a recent analysis of this issue in the special case of aging see Muehlroth and Werkle-Bergner, 2020). We also note that delta power, commonly considered as a marker of slow wave activity and of homeostatically regulated sleep need, does not imply any thresholding, and that small slow waves show clear homeostatic changes as much as (if not more than) larger slow waves (Bernardi et al., 2018; Riedner et al., 2007). In line with these considerations, our analyses showed that small and large slow waves are associated with similar BOLD-signal changes, which were however of greater magnitude for larger EEG slow waves.

Conclusions

Overall, present results indicate that human slow waves of light sleep are associated with complex patterns of hemodynamic changes, including both increases and decreases, and involving cortical as well as subcortical structures. While studies in less disturbed and deeper sleep will be necessary to confirm our findings, the observed patterns of brain activity appear consistent with theoretical accounts of the functions of sleep slow waves. In particular, the strong connectivity between activated thalamic nuclei and limbic structures is consistent with a role of sleep slow waves in memory processing (Miyamoto et al., 2017). Moreover, our results demonstrate coupled electrophysiological and hemodynamic fluctuations that orderly propagate from a preferential origin in centro-frontal cortical brain areas to more anterior and posterior regions. We hypothesize that these coupled propagation dynamics could have a direct role in the generation of gradients of CSF flows and in the clearance of metabolic wastes (Fultz et al., 2019). The mechanism and function of the slow-wave-dependent electrophysiological-hemodynamic coupling undoubtedly deserves future investigations due to its possible implication in pathological conditions.

Data availability

The datasets analyzed in the present study are available from the corresponding author on reasonable request. All relevant cortical and subcortical maps, including main results and parcellations, are available in the OSF public data repository at the following link: https://osf.io/24swv/?view_only=94179de1cdf64049b2b526789ca0f38e.

Declaration of Competing Interests

The authors report no competing interests.

Acknowledgments

This work was supported by intramural funds from the IMT School for Advanced Studies Lucca (to G.B., M.B., G.H., A.L.), the Swiss National Science Foundation (Ambizione Grant PZ00P3_173955 to F.S.), the Divesa Foundation Switzerland (to F.S.), the Pierre-Mercier Foundation for Science (to F.S.), the Bourse Pro-Femme of the University of Lausanne (to F.S.), the Foundation for the University of Lausanne (to F.S and G.B.), an International Brain Research Organization Pan-European Regional Committee short-term postdoctoral fellowship (to G.B.), and a grant “Dipartimenti di Eccellenza 2018–2022”, MIUR-Italy, to the Department of Biomedical, Metabolic and Neural Sciences (S.M. and F.B.). The authors would like to thank Jeff Duyn, Dante Picchioni and Pinar Senay Özbay for their comments and suggestions on a preliminary version of this work.

Author Contributions

Conceptualization: G.B., F.S., G.H., F.B., E.R.; *Data acquisition*: M.B., G.H., A.L., V.F., S.M., D.B., F.B., G.B.; *Data analysis*: M.B., G.H., A.L., A.F., G.B.; *Visualization:* M.B., G.H, G.B.*; Results interpretation*: G.B., M.B., F.S.; *Wrote the manuscript*: G.B., M.B., G.H.; *Revised and edited the manuscript*: All authors.

Supplementary materials

Supplementary material associated with this article can be found, in the online version, at doi:10.1016/j.neuroimage.2021.118117.

References

Allen, P.J., Josephs, O., Turner, R., 2000. A method for removing imaging artifact from continuous EEG recorded during functional MRI. Neuroimage 12, 230–239. doi:10.1006/nimg.2000.0599.

Amzica, F., Steriade, M., 1995. Short- and long-range neuronal synchronization of the slow (<1Hz) cortical oscillation. J. Neurophysiol. 73, 20–38. doi:10.1152/jn.1995.73.1.20.

Andrillon, T., Kouider, S., 2020. The vigilant sleeper: neural mechanisms of sensory (de)coupling during sleep. Curr. Opin. Physiol. 15, 47–59. doi:10.1016/j.cophys.2019.12.002.

Avvenuti, G., Handjaras, G., Betta, M., Cataldi, J., Imperatori, L.S., Lattanzi, S., Riedner, B.A., Pietrini, P., Ricciardi, E., Tononi, G., Siclari, F., Polonara, G., Fabri, M., Silvestrini, M., Bellesi, M., Bernardi, G., 2020. Integrity of corpus callosum is essential for the cross-hemispheric propagation of sleep slow waves: a high-density EEG study in split-brain patients. J. Neurosci. 40, 5589–5603. doi:10.1523/jneurosci.2571-19.2020.

Benjamini, Y., Hochberg, Y., 1995. Controlling the false discovery rate: a practical and powerful approach to multiple testing. J. R. Stat. Soc. Ser. B 57, 289–300. doi:10.1111/j.2517-6161.1995.tb02031.x.

Bernardi, G., Betta, M., Cataldi, J., Leo, A., Haba-Rubio, J., Heinzer, R., Cirelli, C., Tononi, G., Pietrini, P., Ricciardi, E., Siclari, F., 2019a. Visual imagery and visual perception induce similar changes in occipital slow waves of sleep. J. Neurophysiol. 121, 2140–2152. doi:10.1152/jn.00085.2019.

Bernardi, G., Betta, M., Ricciardi, E., Pietrini, P., Tononi, G., Siclari, F., 2019b. Regional delta waves in human rapid eye movement sleep. J. Neurosci. 39, 2686–2697. doi:10.1523/JNEUROSCI.2298-18.2019.

Bernardi, G., Siclari, F., 2019. Local patterns of sleep and wakefulness. Handbook of Behavioral Neuroscience doi:10.1016/B978-0-12-813743-7.00003-7.

Bernardi, G., Siclari, F., Handjaras, G., Riedner, B.A., Tononi, G., 2018. Local and widespread slow waves in stable NREM sleep : evidence for distinct regulation mechanisms. Front. Hum. Neurosci. 12, 1–13. doi:10.3389/fnhum.2018.00248.

Bright, M.G., Tench, C.R., Murphy, K., 2017. Potential pitfalls when denoising resting state fMRI data using nuisance regression. Neuroimage 154, 159–168. doi:10.1016/j.neuroimage.2016.12.027.

Brown, M.B., 1975. A method for combining non-independent, one-sided tests of significance. Biometrics 31, 987. doi:10.2307/2529826.

Brown, R.E., Basheer, R., McKenna, J.T., Strecker, R.E., McCarley, R.W., 2012. Control of sleep and wakefulness. Physiol. Rev. 92, 1087–1187. doi:10.1152/physrev.00032.2011.

Buchmann, A., Kurth, S., Ringli, M., Geiger, A., Jenni, O.G., Huber, R., 2011. Anatomical markers of sleep slow wave activity derived from structural magnetic resonance images. J. Sleep Res. 20, 506–513. doi:10.1111/j.1365-2869.2011.00916.x.

Buckner, R.L., Krienen, F.M., Castellanos, A., Diaz, J.C., Thomas Yeo, B.T., 2011. The organization of the human cerebellum estimated by intrinsic functional connectivity. J. Neurophysiol. 106, 2322–2345. doi:10.1152/jn.00339.2011.

Canto, C.B., Onuki, Y., Bruinsma, B., van der Werf, Y.D., De Zeeuw, C.I., 2017. The sleeping cerebellum. Trends Neurosci. 40, 309–323. doi:10.1016/j.tins.2017.03.001.

Caporro, M., Haneef, Z., Yeh, H.J., Lenartowicz, A., Buttinelli, C., Parvizi, J., Stern, J.M., 2012. Functional MRI of sleep spindles and K-complexes. Clin. Neurophysiol. 123, 303–309. doi:10.1016/j.clinph.2011.06.018.

Cash, S.S., Halgren, E., Dehghani, N., Rossetti, A.O., Thesen, T., Wang, C.M., Devinsky, O., Kuzniecky, R., Doyle, W., Madsen, J.R., Bromfield, E., Eross, L., Halász, P., Karmos, G., Csercsa, R., Wittner, L., Ulbert, I., 2009. The human K-complex represents an isolated cortical down-state. Science 80 (324), 1084–1087. doi:10.1126/science.1169626.

Chang, C., Cunningham, J.P., Glover, G.H., 2009. Influence of heart rate on the BOLD signal: the cardiac response function. Neuroimage 44, 857–869. doi:10.1016/j.neuroimage.2008.09.029.

Colavito, V., Tesoriero, C., Wirtu, A.T., Grassi-Zucconi, G., Bentivoglio, M., 2015. Limbic thalamus and state-dependent behavior: the paraventricular nucleus of the thalamic midline as a node in circadian timing and sleep/wake-regulatory networks. Neurosci. Biobehav. Rev. 54, 3–17. doi:10.1016/j.neubiorev.2014.11.021.

Contreras, D., Steriade, M., 1995. Cellular basis of EEG slow rhythms: a study of dynamic corticothalamic relationships. J. Neurosci. 15, 604–622. doi:10.1523/jneurosci.15-01-00604.1995.

Cox, R., Van Driel, J., De Boer, M., Talamini, L.M., 2014. Slow oscillations during sleep coordinate interregional communication in cortical networks. J. Neurosci. 34, 16890–16901. doi:10.1523/JNEUROSCI.1953-14.2014.

Cox, R.W., 2012. AFNI: what a long strange trip it's been. Neuroimage 62, 743–747. doi:10.1016/j.neuroimage.2011.08.056.

Cox, R.W., 1996. AFNI: software for analysis and visualization of functional magnetic resonance neuroimages. Comput. Biomed. Res. 29, 162–173. doi:10.1006/cbmr.1996.0014.

Crunelli, V., Hughes, S.W., 2010. The slow (1Hz) rhythm of non-REM sleep: a dialogue between three cardinal oscillators. Nat. Neurosci. 13, 9–17. doi:10.1038/nn.2445.

Crunelli, V., Larincz, M.L., Connelly, W.M., David, F., Hughes, S.W., Lambert, R.C., Leresche, N., Errington, A.C., 2018. Dual function of thalamic low-vigilance state oscillations: rhythm-regulation and plasticity. Nat. Rev. Neurosci. 19, 107–118. doi:10.1038/nrn.2017.151.

Czisch, M., Wehrle, R., Stiegler, A., Peters, H., Andrade, K., Holsboer, F., Sämann, P.G., 2009. Acoustic oddball during NREM sleep: a combined EEG/fMRI study. PLoS ONE 4. doi:10.1371/journal.pone.0006749.

Czisch, M., Wetter, T.C., Kaufmann, C., Pollmächer, T., Holsboer, F., Auer, D.P., 2002. Altered processing of acoustic stimuli during sleep: reduced auditory activation and visual deactivation detected by a combined fMRI/EEG study. Neuroimage 16, 251–258. doi:10.1006/nimg.2002.1071.

Dang-Vu, T.T., Schabus, M., Desseilles, M., Albouy, G., Boly, M., Darsaud, A., Gais, S., Rauchs, G., Sterpenich, V., Vandewalle, G., Carrier, J., Moonen, G., Balteau, E., Degueldre, C., Luxen, A., Phillips, C., Maquet, P., 2008. Spontaneous neural activity during human slow wave sleep. Proc. Natl. Acad. Sci. U. S. A. 105, 15160–15165. doi:10.1073/pnas.0801819105.

David, F., Schmiedt, J.T., Taylor, H.L., Orban, G., Di Giovanni, G., Uebele, V.N., Renger, J.J., Lambert, R.C., Leresche, N., Crunelli, V., 2013. Essential thalamic contribution to slow waves of natural sleep. J. Neurosci. 33, 19599–19610. doi:10.1523/JNEUROSCI.3169-13.2013.

De Gennaro, L., Ferrara, M., Bertini, M., 2000. The spontaneous K-complex during stage 2 sleep: is it the "forerunner" of delta waves? Neurosci. Lett. 291, 41–43. doi:10.1016/S0304-3940(00)01366-5.

De Gennaro, L., Gorgoni, M., Reda, F., Lauri, G., Truglia, I., Cordone, S., Scarpelli, S., Mangiaruga, A., D'Atri, A., Lacidogna, G., Ferrara, M., Marra, C., Rossini, P.M., 2017. The fall of sleep K-complex in Alzheimer disease. Sci. Rep. 7. doi:10.1038/srep39688.

Delorme, A., Makeig, S., 2004. EEGLAB: an open source toolbox for analysis of single-trial EEG dynamics including independent component analysis. J. Neurosci. Methods 134, 9–21.

Diedrichsen, J., Balsters, J.H., Flavell, J., Cussans, E., Ramnani, N., 2009. A probabilistic MR atlas of the human cerebellum. Neuroimage 46, 39–46. doi:10.1016/j.neuroimage.2009.01.045.

Diedrichsen, J., Maderwald, S., Küper, M., Thürling, M., Rabe, K., Gizewski, E.R., Ladd, M.E., Timmann, D., 2011. Imaging the deep cerebellar nuclei: a probabilistic atlas and normalization procedure. Neuroimage 54, 1786–1794. doi:10.1016/j.neuroimage.2010.10.035.

Diekelmann, S., Born, J., 2010. The memory function of sleep. Nat. Rev. Neurosci. 11, 114–126. doi:10.1038/nrn2762.

Duyn, J.H., Ozbay, P.S., Chang, C., Picchioni, D., 2020. Physiological changes in sleep that affect fMRI inference. Curr. Opin. Behav. Sci. doi:10.1016/j.cobeha.2019.12.007.

Erdoğan, S.B., Tong, Y., Hocke, L.M., Lindsey, K.P., deB Frederick, B., 2016. Correcting for blood arrival time in global mean regression enhances functional connectivity analysis of resting state fMRI-BOLD signals. Front. Hum. Neurosci. 10. doi:10.3389/fnhum.2016.00311.

Eschenko, O., Magri, C., Panzeri, S., Sara, S.J., 2012. Noradrenergic neurons of the locus coeruleus are phase locked to cortical up-down states during sleep. Cereb. Cortex 22, 426–435. doi:10.1093/cercor/bhr121.

Foerster, B.U., Tomasi, D., Caparelli, E.C., 2005. Magnetic field shift due to mechanical vibration in functional magnetic resonance imaging. Magn. Reson. Med. 54, 1261–1267. doi:10.1002/mrm.20695.

Fonov, V., Evans, A., McKinstry, R., Almli, C., Collins, D., 2009. Unbiased nonlinear average age-appropriate brain templates from birth to adulthood. Neuroimage 47, S102. doi:10.1016/s1053-8119(09)70884-5.

Fultz, N.E., Bonmassar, G., Setsompop, K., Stickgold, R.A., Rosen, B.R., Polimeni, J.R., Lewis, L.D., 2019. Coupled electrophysiological, hemodynamic, and cerebrospinal fluid oscillations in human sleep. Science 80 (366), 628–631.

Funk, C.M., Honjoh, S., Rodriguez, A.V., Cirelli, C., Tononi, G., 2016. Local slow waves in superficial layers of primary cortical areas during REM sleep. Curr. Biol. 26, 396–403.

Gaspar, P., Berger, B., Febvret, A., Vigny, A., Henry, J.P., 1989. Catecholamine innervation of the human cerebral cortex as revealed by comparative immunohistochemistry of tyrosine hydroxylase and dopamine-beta-hydroxylase. J. Comp. Neurol. 279, 249–271. doi:10.1002/cne.902790208.

Gent, T.C., Bandarabadi, M., Herrera, C.G., Adamantidis, A.R., 2018a. Thalamic dual control of sleep and wakefulness. Nat. Neurosci. 21, 974–984. doi:10.1038/s41593-018-0164-7.

Gent, T.C., Bassetti, C.L.A, Adamantidis, A.R., 2018b. Sleep-wake control and the thalamus. Curr. Opin. Neurobiol. 52, 188–197. doi:10.1016/j.conb.2018.08.002.

Hablitz, L.M., Vinitsky, H.S., Sun, Q., Stæger, F.F., Sigurdsson, B., Mortensen, K.N., Lilius, T.O., Nedergaard, M., 2019. Increased glymphatic influx is correlated with high EEG delta power and low heart rate in mice under anesthesia. Sci. Adv. 5, eaav5447. doi:10.1126/sciadv.aav5447.

Halász, P., 2016. The K-complex as a special reactive sleep slow wave - a theoretical update. Sleep Med. Rev. 29, 34–40. doi:10.1016/j.smrv.2015.09.004.

Honjoh, S., Sasai, S., Schiereck, S.S., Nagai, H., Tononi, G., Cirelli, C., 2018. Regulation of cortical activity and arousal by the matrix cells of the ventromedial thalamic nucleus. Nat. Commun. 9. doi:10.1038/s41467-018-04497-x.

Hwang, K., Bertolero, M.A., Liu, W.B., D'Esposito, M., 2017. The human thalamus is an integrative hub for functional brain networks. J. Neurosci. 37, 5594–5607. doi:10.1523/JNEUROSCI.0067-17.2017.

Iannetti, G.D., Niazy, R.K., Wise, R.G., Jezzard, P., Brooks, J.C.W., Zambreanu, L., Vennart, W., Matthews, P.M., Tracey, I., 2005. Simultaneous recording of laser-evoked brain potentials and continuous, high-field functional magnetic resonance imaging in humans. Neuroimage 28, 708–719. doi:10.1016/j.neuroimage.2005.06.060.

Iber, C., Ancoli-Israel, S., Chesson, A., 2007. The AASM Manural for the Scoring of Sleep and Associated Events: Rules, Terminology and Technical Specifications. American Academy of Sleep Medicine, Westchester, IL.

Iriarte, J., Urrestarazu, E., Valencia, M., Alegre, M., Malanda, A., Viteri, C.C., Artieda, J., 2003. Independent component analysis as a tool to eliminate artifacts in EEG: a quantitative study. J. Clin. Neurophysiol. doi:10.1097/00004691-200307000-00004.

Jahnke, K., von Wegner, F., Morzelewski, A., Borisov, S., Maischein, M., Steinmetz, H., Laufs, H., 2012. To wake or not to wake? The two-sided nature of the human K-complex. Neuroimage 59, 1631–1638. doi:10.1016/J.NEUROIMAGE.2011.09.013.

Javoy-Agid, F., Scatton, B., Ruberg, M., L'heureux, R., Cervera, P., Raisman, R., Maloteaux, J.-.M., Beck, H., Agid, Y., 1989. Distribution of monoaminergic, cholinergic, and GABAergic markers in the human cerebral cortex. Neuroscience 29, 251–259. doi:10.1016/0306-4522(89)90055-9.

Lajnef, T., Chaibi, S., Eichenlaub, J.B., Ruby, P.M., Aguera, P.E., Samet, M., Kachouri, A., Jerbi, K., 2015. Sleep spindle and K-complex detection using tunable Q-factor wavelet transform and morphological component analysis. Front. Hum. Neurosci. 9, 1–17. doi:10.3389/fnhum.2015.00414.

Laufs, H., Walker, M.P., Lund, T.E., 2007. 'Brain activation and hypothalamic functional connectivity during human non-rapid eye movement sleep: an EEG/fMRI study'çits limitations and an alternative approach. Brain 130. doi:10.1093/brain/awm084.

Laurino, M., Menicucci, D., Piarulli, A., Mastorci, F., Bedini, R., Allegrini, P., Gemignani, A., 2014. Disentangling different functional roles of evoked K-complex components: mapping the sleeping brain while quenching sensory processing. Neuroimage 86, 433–445.

Laurino, M., Piarulli, A., Menicucci, D., Gemignani, A., 2019. Local gamma activity during non-REM sleep in the context of sensory evoked K-complexes. Front. Neurosci. 13. doi:10.3389/fnins.2019.01094.

Lemieux, M., Chen, J.Y., Lonjers, P., Bazhenov, M., Timofeev, I., 2014. The impact of cortical deafferentation on the neocortical slow oscillation. J. Neurosci. 34, 5689–5703. doi:10.1523/JNEUROSCI.1156-13.2014.

Lewis, D.A., Morrison, J.H., 1989. Noradrenergic innervation of monkey prefrontal cortex: a dopamine-β-hydroxylase immunohistochemical study. J. Comp. Neurol. 282, 317–330. doi:10.1002/cne.902820302.

Lőrincz, M.L., Gunner, D., Bao, Y., Connelly, W.M., Isaac, J.T.R., Hughes, S.W., Crunelli, V., 2015. A distinct class of slow (~0.2–2Hz) intrinsically bursting layer 5 pyramidal neurons determines UP/DOWN state dynamics in the neocortex. J. Neurosci. 35, 5442–5458. doi:10.1523/JNEUROSCI.3603-14.2015.

Mander, B.A., Marks, S.M., Vogel, J.W., Rao, V., Lu, B., Saletin, J.M., Ancoli-Israel, S., Jagust, W.J., Walker, M.P., 2015. β-amyloid disrupts human NREM slow waves and related hippocampus-dependent memory consolidation. Nat. Neurosci. 18, 1051–1057. doi:10.1038/nn.4035.

Massimini, M., Huber, R., Ferrarelli, F., Hill, S., Tononi, G., 2004. The sleep slow oscillation as a traveling wave. J. Neurosci. 24, 6862–6870. doi:10.1523/JNEUROSCI.1318-04.2004.

Mena-segovia, J., Sims, H.M., Magill, P.J., Bolam, J.P., 2008. Cholinergic brainstem neurons modulate cortical gamma activity during slow oscillations. J. Physiol. 586, 2947–2960. doi:10.1113/jphysiol.2008.153874.

Menicucci, D., Piarulli, A., Debarnot, U., d'Ascanio, P., Landi, A., Gemignani, A., 2009. Functional structure of spontaneous sleep slow oscillation activity in humans. PLoS ONE 4, e7601.

Mensen, A., Poryazova, R., Huber, R., Bassetti, C.L., 2018. Individual spindle detection and analysis in high-density recordings across the night and in thalamic stroke. Sci. Rep. 8. doi:10.1038/s41598-018-36327-x.

Mensen, A., Riedner, B., Tononi, G., 2016. Optimizing detection and analysis of slow waves in sleep EEG. J. Neurosci. Methods 274, 1–12. doi:10.1016/j.jneumeth.2016.09.006.

Mitra, A., Snyder, A.Z., Tagliazucchi, E., Laufs, H., Raichle, M.E., 2015. Propagated infra-slow intrinsic brain activity reorganizes across wake and slow wave sleep. Elife 4. doi:10.7554/elife.10781.

Miyamoto, D., Hirai, D., Murayama, M., 2017. The roles of cortical slow waves in synaptic plasticity and memory consolidation. Front. Neural Circ. 11. doi:10.3389/fncir.2017.00092.

Moruzzi, G., Magoun, H.W.W., 1949. Brain stem reticular formation and activation of the EEG. Electroencephalogr. Clin. Neurophysiol. 1, 455–473. doi:10.1016/0013-4694(49)90219-9.

Mountcastle, V.B., Poggio, G.F., 1974. Structural organization and general physiology of thalamotelencephalic systems. In: Medical Physiology. CV Mosby Co St. Louis, pp. 227–253.

Muehlroth, B.E., Werkle-Bergner, M., 2020. Understanding the interplay of sleep and aging: methodological challenges. Psychophysiology e13523. https://doi.org/10.1111/psyp.13523

Mullinger, K., Bowtell, R., 2010. Combining EEG and fMRI. Methods Mol. Biol. 711, 303–326. doi:10.1007/978-1-61737-992-5_15.

Murphy, M., Riedner, B.A., Huber, R., Massimini, M., Ferrarelli, F., Tononi, G., 2009. Source modeling sleep slow waves. Proc. Natl. Acad. Sci. U. S. A. 106, 1608–1613. doi:10.1073/pnas.0807933106.

Najdenovska, E., Alemán-Gómez, Y., Battistella, G., Descoteaux, M., Hagmann, P., Jacquemont, S., Maeder, P., Thiran, J.P., Fornari, E., Cuadra, M.B., 2018. In-vivo probabilistic atlas of human thalamic nuclei based on diffusion-weighted magnetic resonance imaging. Sci. Data 5. doi:10.1038/sdata.2018.270.

Neske, G.T., 2016. The slow oscillation in cortical and thalamic networks: mechanisms and functions. Front. Neural Circ. 9. doi:10.3389/fncir.2015.00088.

Niazy, R.K., Beckmann, C.F., Iannetti, G.D., Brady, J.M., Smith, S.M., 2005. Removal of FMRI environment artifacts from EEG data using optimal basis sets. Neuroimage 28, 720–737. doi:10.1016/j.neuroimage.2005.06.067.

Nierhaus, T., Gundlach, C., Goltz, D., Thiel, S.D., Pleger, B., Villringer, A., 2013. Internal ventilation system of MR scanners induces specific EEG artifact during simultaneous EEG-fMRI. Neuroimage 74, 70–76. doi:10.1016/j.neuroimage.2013.02.016.

Özbay, P.S., Chang, C., Picchioni, D., Mandelkow, H., Chappel-Farley, M.G., van Gelderen, P., de Zwart, J.A., Duyn, J., 2019. Sympathetic activity contributes to the fMRI signal. Commun. Biol. doi:10.1038/s42003-019-0659-0.

Piantoni, G., Poil, S.-.S., Linkenkaer-Hansen, K., Verweij, I.M., Ramautar, J.R., Van Someren, E.J.W., Van Der Werf, Y.D., 2013. Individual differences in white matter diffusion affect sleep oscillations. J. Neurosci. 33, 227–233. doi:10.1523/jneurosci.2030-12.2013.

Poulet, J.F.A., Fernandez, L.M.J., Crochet, S., Petersen, C.C.H., 2012. Thalamic control of cortical states. Nat. Neurosci. 15, 370–372. doi:10.1038/nn.3035.

Riedner, B.A., Hulse, B.K., Murphy, M.J., Ferrarelli, F., Tononi, G., 2011. Temporal dynamics of cortical sources underlying spontaneous and peripherally evoked slow waves. Prog. Brain Res. 193, 201.

Riedner, B.A., Vyazovskiy, V.V., Huber, R., Massimini, M., Esser, S., Murphy, M., Tononi, G., 2007. Sleep homeostasis and cortical synchronization: III. A high-density EEG study of sleep slow waves in humans. Sleep 30, 1643.

Romero, S., Mailanas, M.a, Clos, S., Gimenez, S., Barbanoj, M.J., 2003. Reduction of EEG artifacts by ICA in different sleep stages. IEEE Int. Conf. Eng. Med. Biol. doi:10.1109/IEMBS.2003.1280467.

Roš, H., Sachdev, R.N.S., Yu, Y., Šestan, N., McCormick, D.A., 2009. Neocortical networks entrain neuronal circuits in cerebellar cortex. J. Neurosci. 29, 10309–10320. doi:10.1523/JNEUROSCI.2327-09.2009.

Rowland, N.C., Goldberg, J.A., Jaeger, D., 2010. Cortico-cerebellar coherence and causal connectivity during slow-wave activity. Neuroscience 166, 698–711. doi:10.1016/j.neuroscience.2009.12.048.

Sanchez-Vives, M.V., McCormick, D.A., 2000. Cellular and network mechanisms of rhythmic recurrent activity in neocortex. Nat. Neurosci. 3, 1027–1034. doi:10.1038/79848.

Schabus, M., Dang-Vu, T.T., Albouy, G., Balteau, E., Boly, M., Carrier, J., Darsaud, A., Degueldre, C., Desseilles, M., Gais, S., Phillips, C., Rauchs, G., Schnakers, C., Sterpenich, V., Vandewalle, G., Luxen, A., Maquet, P., 2007. Hemodynamic cerebral correlates of sleep spindles during human non-rapid eye movement sleep. Proc. Natl. Acad. Sci. U. S. A. doi:10.1073/pnas.0703084104.

Schaefer, A., Kong, R., Gordon, E.M., Laumann, T.O., Zuo, X.-.N., Holmes, A.J., Eickhoff, S.B., Yeo, B.T.T., 2018. Local-global parcellation of the human cerebral cortex from intrinsic functional connectivity MRI. Cereb. Cortex 28, 3095–3114. doi:10.1093/cercor/bhx179.

Schweimer, J.V., Mallet, N., Sharp, T., Ungless, M.A., 2011. Spike-timing relationship of neurochemically-identified dorsal raphe neurons during cortical slow oscillations. Neuroscience 196, 115–123. doi:10.1016/j.neuroscience.2011.08.072.

Sheroziya, M., Timofeev, I., 2014. Global intracellular slow-wave dynamics of the thalamocortical system. J. Neurosci. 34, 8875–8893. doi:10.1523/JNEUROSCI.4460-13.2014.

Siclari, F., Bernardi, G., Cataldi, J., Tononi, G., 2018. Dreaming in NREM sleep: a high-density EEG study of slow waves and spindles. J. Neurosci. 38. doi:10.1523/JNEUROSCI.0855-18.2018, 0855–18.

Siclari, F., Bernardi, G., Riedner, B.A., LaRocque, J.J., Benca, R.M., Tononi, G., 2014. Two distinct synchronization processes in the transition to sleep: a high-density electroencephalographic study. Sleep 37, 1621–1637. doi:10.5665/sleep.4070.

Slézia, A., Hangya, B., Ulbert, I., Acsády, L., 2011. Phase advancement and nucleus-specific timing of thalamocortical activity during slow cortical oscillation. J. Neurosci. 31, 607–617. doi:10.1523/JNEUROSCI.3375-10.2011.

Steriade, M., Aposto, V., Oakson, G., 1971a. Clustered firing in the cerebellothalamic pathway during synchronized sleep. Brain Res 26, 425–432. doi:10.1016/S0006-8993(71)80020-3.

Steriade, M., Apostol, V., Oakson, G., 1971b. Control of unitary activities in cerebellothalamic pathway during wakefulness and synchronized sleep. J. Neurophysiol. 34, 389–413. doi:10.1152/jn.1971.34.3.389.

Steriade, M., Glenn, L.L., 1982. Neocortical and caudate projections of intralaminar thalamic neurons and their synaptic excitation from midbrain reticular core. J. Neurophysiol. 48, 352–371. doi:10.1152/jn.1982.48.2.352.

Steriade, M., Nunez, A., Amzica, F., 1993a. A novel slow (< 1Hz) oscillation of neocortical neurons in vivo: depolarizing and hyperpolarizing components. J. Neurosci. 13, 3252–3265. doi:10.1523/jneurosci.13-08-03252.1993.

Steriade, M., Nunez, A., Amzica, F., 1993b. Intracellular analysis of relations between the slow (<1Hz) neocortical oscillation and other sleep rhythms of the electroencephalogram. J. Neurosci. 13, 3266–3283. doi:10.1523/jneurosci.13-08-03266.1993.

Thomas Yeo, B.T., Krienen, F.M., Sepulcre, J., Sabuncu, M.R., Lashkari, D., Hollinshead, M., Roffman, J.L., Smoller, J.W., Zöllei, L., Polimeni, J.R., Fisch, B., Liu, H., Buckner, R.L., 2011. The organization of the human cerebral cortex estimated by intrinsic functional connectivity. J. Neurophysiol. 106, 1125–1165. doi:10.1152/jn.00338.2011.

Timofeev, I., Chauvette, S., 2017. Sleep slow oscillation and plasticity. Curr. Opin. Neurobiol. 44, 116–126. doi:10.1016/j.conb.2017.03.019.

Timofeev, I., Grenier, F., Bazhenov, M., Sejnowski, T.J., Steriade, M., Timofeev, I., Grenier, F., Bazhenov, M., Sejnowski, T.J., Steriade, M., 2000. Origin of slow cortical oscillations in deafferented cortical slabs. Cereb. Cortex 10, 1185–1199.

Timofeev, I., Schoch, S.F., LeBourgeois, M.K., Huber, R., Riedner, B.A., Kurth, S., 2020. Spatio-temporal properties of sleep slow waves and implications for development. Curr. Opin. Physiol. 15, 172–182. doi:10.1016/j.cophys.2020.01.007.

Timofeev, I., Steriade, M., 1996. Low-frequency rhythms in the thalamus of intact-cortex and decorticated cats. J. Neurophysiol. 76, 4152–4168. doi:10.1152/jn.1996.76.6.4152.

Tononi, G., Cirelli, C., 2014. Sleep and the price of plasticity: from synaptic and cellular homeostasis to memory consolidation and integration. Neuron 81, 12–34. doi:10.1016/j.neuron.2013.12.025.

Ushimaru, M., Kawaguchi, Y., 2015. Temporal structure of neuronal activity among cortical neuron subtypes during slow oscillations in anesthetized rats. J. Neurosci. 35, 11988–12001. doi:10.1523/JNEUROSCI.5074-14.2015.

Valomon, et al., 2021. A high-density electroencephalography study reveals abnormal sleep homeostasis in patients with rapid eye movement sleep behavior disorder. Scientific Reports doi:10.1038/s41598-021-83980-w.

van der Meer, J.N., Pampel, A., Van Someren, E.J.W., Ramautar, J.R., van der Werf, Y.D., Gomez-Herrero, G., Lepsien, J., Hellrung, L., Hinrichs, H., Möller, H.E., Walter, M., 2016. Carbon-wire loop based artifact correction outperforms post-processing EEG/fMRI corrections-A validation of a real-time simultaneous EEG/fMRI correction method. Neuroimage 125, 880–894. doi:10.1016/j.neuroimage.2015.10.064.

Vertes, R.P., Linley, S.B., Hoover, W.B., 2015. Limbic circuitry of the midline thalamus. Neurosci. Biobehav. Rev. 54, 89–107. doi:10.1016/j.neubiorev.2015.01.014.

Wamsley, E.J., Tucker, M.A., Shinn, A.K., Ono, K.E., McKinley, S.K., Ely, A.V., Goff, D.C., Stickgold, R., Manoach, D.S., 2012. Reduced sleep spindles and spindle coherence in schizophrenia: mechanisms of impaired memory consolidation? Biol. Psychiatry 71, 154–161. doi:10.1016/j.biopsych.2011.08.008.

Xie, L., Kang, H., Xu, Q., Chen, M.J., Liao, Y., Thiyagarajan, M., O'Donnell, J., Christensen, D.J., Nicholson, C., Iliff, J.J., 2013. Sleep drives metabolite clearance from the adult brain. Science 80 (342), 373–377.